Ensemble hydrological prediction-based real-time optimization of a multiobjective reservoir during flood season in a semiarid basin with global numerical weather predictions

Fuxing Wang,[1,2,3] Lei Wang,[2,3] Huicheng Zhou,[1] Oliver C. Saavedra Valeriano,[4,5] Toshio Koike,[3] and Wenlong Li[6]

Received 6 September 2011; revised 13 May 2012; accepted 12 June 2012; published 25 July 2012.

[1] Future streamflow uncertainties hinder reservoir real-time operation, but the ensemble prediction technique is effective for reducing the uncertainties. This study aims to combine ensemble hydrological predictions with real-time multiobjective reservoir optimization during flood season. The ensemble prediction-based reservoir optimization system (EPROS) takes advantage of 8 day lead time global numerical weather predictions (NWPs) by the Japan Meteorological Agency (JMA). Thirty-member ensemble streamflows are generated through running the water and energy budget-based distributed hydrological model fed with 30-member perturbed quantitative precipitation forecasts (QPFs) and deterministic NWPs. The QPF perturbation amplitudes are calculated from the QPF intensity and location errors during previous 8 day periods. The reservoir objective function is established to minimize the maximum reservoir water level (reservoir and upstream safety), the downstream flood peak (downstream safety), and the difference between simulated reservoir end water level and target level (water use). The system is evaluated on the Fengman reservoir basin (semiarid), which often suffers from extreme floods in summer and serious droughts in spring. The results show the ensemble QPFs generated by EPROS are comparable to those for JMA by using probability-based measures. The streamflow forecast error is significantly reduced by employing the ensemble prediction approach. The system has demonstrated high efficiency in optimizing reservoir objectives for both normal and critical flood events. Fifty-member ensembles generate a wider streamflow and reservoir release range than 10-member ensembles, but the ensemble mean end water levels and releases are comparable. The system is easy to operate and thereby feasible for practical operations in various reservoir basins.

Citation: Wang, F., L. Wang, H. Zhou, O. C. Saavedra Valeriano, T. Koike, and W. Li (2012), Ensemble hydrological prediction-based real-time optimization of a multiobjective reservoir during flood season in a semiarid basin with global numerical weather predictions, *Water Resour. Res.*, *48*, W07520, doi:10.1029/2011WR011366.

1. Introduction

[2] The climate change induced frequent floods [*Intergovernmental Panel on Climate Change*, 2007] and the continuous increase of water demand [*Clark and Hay*, 2004] show the need to manage water resources appropriately [*Cai et al.*, 2003]. Reservoir plays a key role in water resources management through optimal operation [*Labadie*, 2004]. The reservoir optimization problems are characterized by multiple objectives and constraints, nonlinear optimization and high dimensionality [*Kumar and Reddy*, 2006; *Yeh*, 1985]. In order to solve such complex problems, a variety of optimization algorithms [e.g., *Stedinger et al.*, 1984; *Yeh*, 1985; *Labadie*, 2004; *Johnson et al.*, 1991; *Goldberg*, 1989; *Oliveira and Loucks*, 1997; *Kennedy and Eberhart*, 1995; *Dorigo et al.*, 1996; *Duan et al.*, 1992, 1993, 1994] and multiple objective handling techniques [*Croley and Raja Rao*, 1979; *Yeh and Becker*, 1982; *Khu and Madsen*, 2005; *Ngo et al.*, 2007; *Reddy and Kumar*, 2007] have been widely employed. With the availability of real-time data and the improvement of computational power, the researches on real-time reservoir optimization models also appear for optimizing real-time release [e.g., *Niewiadomska-Szynkiewicz et al.*, 1996; *Chang et al.*, 2005; *Hsu and Wei*, 2007; *Ngo et al.*, 2007; *Saavedra Valeriano et al.*, 2010a, 2010b]. Although considerable promising results are

[1]Institute of Water Resources and Flood Control, Dalian University of Technology, Dalian, China.
[2]Key Laboratory of Tibetan Environment Changes and Land Surface Processes, Institute of Tibetan Plateau Research, Chinese Academy of Sciences, Beijing, China.
[3]Department of Civil Engineering, University of Tokyo, Tokyo, Japan.
[4]Department of Civil and Environmental Engineering, Tokyo Institute of Technology, Tokyo, Japan.
[5]Energy Resources and Environmental Engineering Program, Egypt-Japan University of Science and Technology, New Borg El-Arab, Egypt.
[6]Fengman Hydropower Plant, Jilin, China.

Corresponding author: F. Wang, Institute of Water Resources and Flood Control, Dalian University of Technology, 2 Linggong Rd., Ganjingzi District, Dalian, 116024, China. (wangfuxings@gmail.com)

0043-1397/12/2011WR011366

obtained and progress has been made, the process of practical real-time operation remains very slow [*Chang et al.*, 2005; *Labadie*, 2004; *Yeh*, 1985] because of the uncertainties of future streamflow [*Tejada-Guibert et al.*, 1995; *You and Cai*, 2008], and the complexity of the systems for the actual reservoir operators [*Russell and Campbell*, 1996].

[3] The uncertainties in precipitation are the main source of uncertainties for streamflow prediction [*Roulin and Vannitsem*, 2005; *Mascaro et al.*, 2010; *Saavedra Valeriano et al.*, 2010a]. Although the accuracy of weather forecasting has improved in past years, the medium-range quantitative precipitation forecast (QPF) in basin scale has been still difficult to predict since the atmosphere is highly unstable [*Roulin and Vannitsem*, 2005; *Saavedra Valeriano et al.*, 2010a]. In order to apply medium-range QPFs for reservoir real-time operation, it is necessary to take into account the QPF errors [*Cui et al.*, 2011; *Fan and van den Dool*, 2011]. In recent decades, many efforts have been made on ensemble forecasting technique to account for the uncertainties (or bias) in meteorological predictions [e.g., *Toth and Kalnay*, 1993, 1997; *Buizza and Palmer*, 1995; *Molteni et al.*, 1996; *Houtekamer et al.*, 1996; *Hamill et al.*, 2000; *Buizza et al.*, 2005; *Schaake et al.*, 2007] and hydrological predictions [e.g., *Day*, 1985; *Clark et al.*, 2004; *Clark and Hay*, 2004; *Werner et al.*, 2005; *Roulin and Vannitsem*, 2005; *Schaake et al.*, 2006; *Dietrich et al.*, 2008; *Cloke and Pappenberger*, 2009; *Pappenberger and Buizza*, 2009; *Mascaro et al.*, 2010; *Wu et al.*, 2011]. The ensemble prediction approach shows great potential for improving predictability and extending lead time through generating multiple predictions for the same location and time [*Cloke and Pappenberger*, 2009; *Thielen et al.*, 2009; *Faber and Stedinger*, 2001]. However, the effective use of ensemble predictions for operational decision making (e.g., reservoir operation) is still a challenge [*Krzysztofowicz*, 2001; *Ramos et al.*, 2007].

[4] In recent decades, several studies were carried out on reservoir optimization using ensemble predictions. *Faber and Stedinger* [2001] employed monthly ensemble streamflow predictions based on historical weather patterns for reservoir operation by using sampling stochastic dynamic programming. *Saavedra Valeriano et al.* [2010a] studied reservoir optimization by taking into account the error distribution of QPFs with 18 h lead time. However, no works have been done on generating ensemble reservoir status (water levels and releases) by employing real-time ensemble hydrological predictions, which are effective for conveying forecast uncertainties to decision makers. The objective of this study is to embed ensemble streamflow predictions into real-time reservoir optimization model for improving reservoir operation during flood season. This combination would benefit both real-time water resources management and the practical application of ensemble predictions.

[5] The ensemble prediction-based reservoir optimization system (EPROS) is presented in this study by improving the prototype of the dam release support system (DRESS [*Saavedra Valeriano et al.*, 2010a]). The EPROS is fed with real-time 8 day global numerical weather predictions (NWPs) obtained from the Japan Meteorological Agency (JMA). The main improvements of the present work can be summarized as follows. First, the QPF intensity error evaluation method is improved to describe the errors comprehensively. The definition of QPF perturbation weight is simplified by using mathematical functions instead of using proposed zones and a look up table. Second, the performance of ensemble QPFs generated by EPROS is compared with JMA's operational ensemble NWPs using probability-based measures (e.g., Continuous Rank Probability Score and Rank Histogram). Third, the hydrological model (water and energy budget-based distributed hydrological model, WEB-DHM) is revised by updating the hydrological status at each time step continuously. This improvement makes the WEB-DHM more flexible and effective for reservoir real-time operation than that used in DRESS. Fourth, the reservoir optimization model is improved. A new measure (reservoir and upstream flood control safety) is added since the upstream cities and reservoir are dangers when the reservoir water level is high. The objective function is then normalized to the same magnitude order to keep the stability of multiobjective optimization. The release constraint is also considered because the dramatic changes in reservoir release may cause damages to the downstream channels and turbine. The dynamic penalty function approach is applied for solving multiconstraint optimization problem. Fifth, the NWPs used in the DRESS [*Saavedra Valeriano et al.*, 2010a] only include QPF, while the predicted winds (zonal and meridional), air temperature, relative humidity, and surface pressure are also embedded into EPROS. The EPROS fed with global scale forecasts makes it feasible to be applied to other river basins in the world. Sixth, the ensemble reservoir status (water levels and releases) and inflows are generated by EPROS, which provides reasonable reference for real-time decision making. Seventh, the sensitivity of reservoir efficiency to ensemble size, and the reservoir performance under critical events are investigated through applying the EPROS for Fengman reservoir (northeast China) within a semiarid basin. The continental semiarid basin having most part of annual precipitation concentrated in July and August, tends to suffer from extreme floods. In the nonflood seasons (from October to May), this region suffers from long-term serious water shortage problem particularly in spring.

[6] This paper is organized as follows. Section 2 describes the general structure of EPROS system, the QPF perturbation approach, the WEB-DHM, and the reservoir optimization model. The study region (northeast China) and data sets are introduced in section 3. Section 4 presents the EPROS system application results for 2004 and 2005 flood events. Section 5 discusses the sensitivity to ensemble size, the model applicability under critical case, and the model feasibility for practical application. Conclusions are given in section 6.

2. Methods

[7] The EPROS is composed of three modules which are the QPF perturbation model, the hydrological prediction model, and the reservoir optimization model. The perturbed QPFs [*Saavedra Valeriano et al.*, 2010a] are calculated according to the recent 8 day QPF intensity and location errors. The perturbed QPFs and NWP outputs (near-surface air temperature, wind speed, air pressure, and relative humidity) then force the WEB-DHM [*Wang et al.*, 2009a, 2009b, 2009c] to generate ensemble streamflows. The reservoir optimization model fed with ensemble streamflows

is running to minimize the maximum reservoir water level and the downstream flood peak, as well as to minimize the difference between optimized and target reservoir water level at the end of optimization. The dynamic penalty function techniques [*Yeniay*, 2005; *Barakat and Ibrahim*, 2011] and the shuffled complex evolution method developed at the University of Arizona (SCE-UA) [*Duan et al.*, 1992, 1993, 1994] is employed to solve multiple constraints and to search for optimal solutions, respectively.

2.1. General Structure of EPROS

[8] The EPROS system structure is presented in Figure 1. There are six steps, and they are summarized as follows.

[9] 1. The QPFs are evaluated with observations by considering the intensity and spatial distribution errors over the past 8 days ($t - 8 \le i \le t - 1$). The performance of the QPFs is represented by weight (w).

[10] 2. Perturbed QPF members are generated during lead time T_{ld} when QPFs are issued ($t \le i \le T_{ld}$). The perturbation range is calculated according to w in step 1.

[11] 3. WEB-DHM is running by using perturbed QPF to predict ensemble dam inflows Qin_i ($t \le i \le T_{ld}$).

[12] 4. The dam optimization model is running to obtain the optimized forecast dam releases $Qout_i$ ($t \le i \le T_{ld}$). The actual dam release at current time step is equal to the optimized forecast dam releases. The dam water volume V_i is transferred to V_{i+1} by using water balance equation. The dam water level (H_i) is interpolated from V_i using the cubic Lagrange interpolation method.

[13] 5. The WEB-DHM forced by observed forcing data is running at the end of the current dam operation step ($i = t$) in order to update initial conditions for the next optimization loop.

[14] 6. If terminate conditions (e.g., optimal solutions are found or at the end of flood season) are satisfied, then the system stopped; otherwise, steps 1 to 5 are repeated. The models employed in steps 1–2, 3 (and 5), and 4 are elaborated in sections 2.2–2.4, respectively.

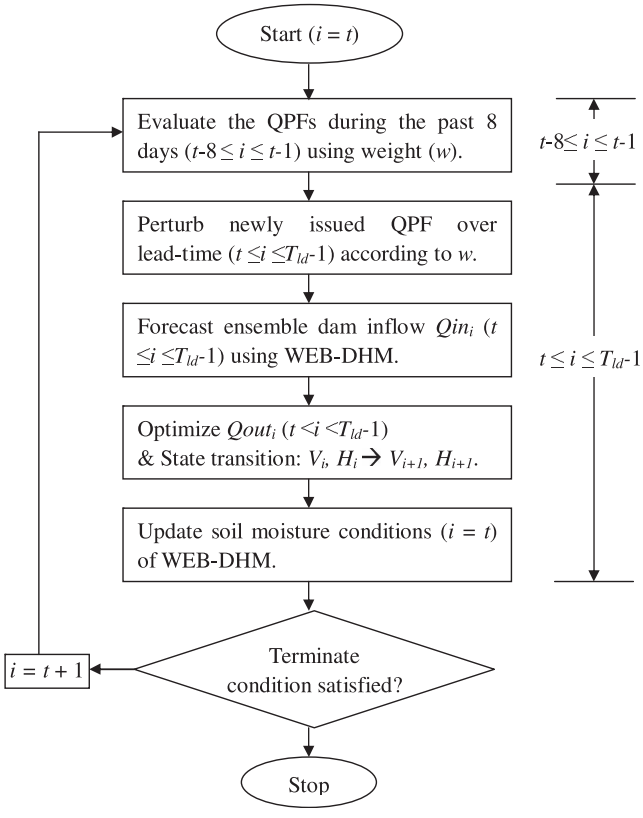

Figure 1. Flowchart of the ensemble prediction-based reservoir optimization system (EPROS). The lead time (T_{ld}) is 8 days.

2.2. QPF Perturbation Model

[15] The perturbed QPFs generation method is based on the concept of *Saavedra Valeriano et al.* [2010a] but improvements are made on perturbation w calculating. *Saavedra Valeriano et al.* [2010a] defined w from a look up table by considering the QPF intensity errors (FE) evaluated at different proposed zones during the previous time step.

$$FE = \frac{1}{2}\left(\frac{HI_{\mathrm{QPF}}}{HI_{\mathrm{OBS}}} + \frac{MI_{\mathrm{QPF}}}{MI_{\mathrm{OBS}}}\right), \tag{1}$$

where HI and MI represent high intensity and mean intensity, respectively. QPF and OBS indicate forecasts and observations, respectively. A very accurate forecast is assumed if the FE is close to 1. FE higher than 1 (between 0 and 1) indicates that the QPF is overestimated (underestimation). According to this definition, the accurate forecast ($FE \approx 1$) may be falsely detected if the HI is underestimated (overestimated) while the MI is overestimated (underestimated) (e.g., $\frac{HI_{\mathrm{QPF}}}{HI_{\mathrm{OBS}}} = 0.6$, $\frac{MI_{\mathrm{QPF}}}{MI_{\mathrm{OBS}}} = 1.4$, $FE = 1$). Moreover, the look up table and the proposed zones are defined subjectively, and they depend on the experience of the user. To reduce subjectivity and increase simplicity, the w in this study is defined as a function of intensity error (e_{itn}) and spatial distribution error (e_{dis}) within the basin during the previous i time step ($t - 8 \le i \le t - 1$; Figure 1). The differences between the QPFs and the observations are considered in order to avoid the false detection of the accurate forecast,

$$w_i = \frac{1}{2}(e_{\mathrm{itn},i} + e_{\mathrm{dis},i}), \tag{2}$$

$$e_{\mathrm{itn},i} = \frac{1}{2}\left[\frac{|I_{F,\max,i} - I_{O,\max,i}|}{\max(I_{F,\max,i}, I_{O,\max,i})} + \frac{|I_{F,\mathrm{mean},i} - I_{O,\mathrm{mean},i}|}{\max(I_{F,\mathrm{mean},i}, I_{O,\mathrm{mean},i})}\right], \tag{3}$$

$$e_{\mathrm{dis}} = \frac{D(L_{F,\max,i}, L_{O,\max,i})}{\max(D)}, \tag{4}$$

where w_i is the weights evaluated at previous time step i, $I_{F,\max,i}$ ($I_{O,\max,i}$) and $I_{F,\mathrm{mean},i}$ ($I_{O,\mathrm{mean},i}$) are maximum and mean intensities of QPF (observation) in the basin, $L_{F,\max,i}$ and $L_{O,\max,i}$ are the maximum rainfall locations (or geometrical center) of QPF and observation in the basin, and D refers to distance and max(D) is the maximum distance

within the basin. The w oscillates between 0 and 1. The lower w is, the better the QPF performed. A perfect QPF should have w equal to 0. The following two special cases of equation (3) are defined:

$$\frac{|I_{F,\max,i} - I_{O,\max,i}|}{\max(I_{F,\max,i}, I_{O,\max,i})} = 0, \ \max(I_{F,\max,i}, I_{O,\max,i}) = 0, \quad (5)$$

$$\frac{|I_{F,\mathrm{mean},i} - I_{O,\mathrm{mean},i}|}{\max(I_{F,\mathrm{mean},i}, I_{O,\mathrm{mean},i})} = 0, \ \max(I_{F,\mathrm{mean},i}, I_{O,\mathrm{mean},i}) = 0, \quad (6)$$

[16] The perturbed [see *Saavedra Valeriano et al.*, 2010a; *Turner et al.*, 2008] QPF (P_QPF) for each model grid (x, y) and for each lead time step i ($t \le i \le 7$; Figure 1) is then calculated from

$$\mathrm{P\_QPF}_i(x,y) = \max\{\mathrm{QPF}_i(x,y)[1 + w_i \times N(0,1)], 0\}, \quad (7)$$

where $N(0, 1)$ is normal distribution with zero mean and a standard deviation of unity. In this way, the perturbed QPF is estimated from the intensity (e_{itn}) and distribution (e_{dis}) errors in the previous time step. The better the QPF performed (i.e., the lower w is), the smaller range of the P_QPF is generated.

2.3. The WEB-DHM Model

[17] The WEB-DHM [*Wang et al.*, 2009a, 2009b, 2009c] was developed by fully coupling a simple biosphere scheme (SiB2) [*Sellers et al.*, 1996a, 1996b] with a geomorphology-based hydrological model (GBHM) [*Yang et al.*, 2002, 2004a]. It can give consistent descriptions of water, energy and CO_2 fluxes in a basin scale. The land surface submodel (the hydrologically improved SiB2 [*Wang et al.*, 2009c]) is used to describe the turbulent fluxes (energy, water and CO_2) between the atmosphere and land surface for each model cell. The hydrological submodel simulates both surface and subsurface runoff, and then calculates flow routing in the river network. A complete description of WEB-DHM was given by *Wang et al.* [2009a, 2009b, 2009c].

[18] In the EPROS, the WEB-DHM model is improved in hydrological status updating method. The WEB-DHM is running before flood events and during flood events, respectively. Before the flood event (e.g., from 1 January to flood event), WEB-DHM is driven by observed atmospheric forcing data in order to achieve hydrological equilibrium. During the flood event, the WEB-DHM is running continuously which includes both forecast run and observation run. WEB-DHM is driven by forecast forcing data during forecast run in order to predict dam inflows during the lead time (e.g., $t \le i \le t + 7$; Figure 1). During observation run, WEB-DHM is driven by observed forcing data at the end of each dam operation step (e.g., $i = t$; Figure 1) in order to update soil initial conditions for the forecast run. In this way, the hydrological status (the soil initial conditions) is updated continuously at each time step with the flow of reservoir optimization. The merit of this improvement is that the WEB-DHM model used in EPROS model is more flexible and effective than that used in DRESS.

2.4. Dam Optimization Model

2.4.1. Objective Function

[19] *Saavedra Valeriano et al.* [2010a, 2010b] established the objective function by minimizing the flood volume at downstream control points (potential flood volume, PFV) and maximizing reservoir storage (reservoir free volume, RFV). The PFV and RFV would be difficult to coordinate if there is high discrepancy in the magnitude order of the two objectives. In this case, the term with higher magnitude would be given preference. In addition, the reservoir (and upstream) flood control safety is also essential for actual reservoir operation [*Wang et al.*, 1994]. The upstream cities are dangerous when the reservoir water level is high, and the loss of life and property is inestimable if the dam break flood occurred. Therefore, three objectives representing reservoir (and upstream) flood control safety ($f_{fc,r}$), downstream flood control safety ($f_{fc,d}$) and future water use (f_{wu}) are optimized in EPROS [*Wang et al.*, 1994]. Parameters $f_{fc,r}$ and $f_{fc,d}$ are defined by minimizing the maximum reservoir water level and minimizing the flood peak at a selected downstream control point, respectively. Parameter f_{wu} is represented by minimizing the discrepancy between the optimized water level and target water level at the end of optimization. The three objectives are expressed as

$$f_{fc,r} = \min\{\max(H_i)\}, 1 \le i \le T, \quad (8)$$

$$f_{fc,d} = \min\{\max(Qctl_i)\}, 1 \le i \le T, \quad (9)$$

$$f_{wu} = \min\{H_T - H_{\mathrm{target}}\}, \quad (10)$$

where T is the total time step (days), H_i is reservoir water level during time period i (m), $Qctl_i$ is river discharge at the control point ($m^3\ s^{-1}$), and H_T and H_{target} are the end and target reservoir water levels (m), respectively. These three objectives are then normalized to same magnitude order.

$$f_{fc,r} = \min\{\max(H_i)/H_{\mathrm{lmt}}\}, 1 \le i \le T, \quad (11)$$

$$f_{fc,d} = \min\{\max(Qctl_i)/Qctl_{\max}\}, 1 \le i \le T, \quad (12)$$

$$f_{wu} = \min\{|H_T - H_{\mathrm{target}}|/|H_{\mathrm{dead}} - H_{\mathrm{target}}|\}, \quad (13)$$

where H_{lmt} and H_{dead} are limited and dead reservoir water levels (m), $Qctl_{\max}$ is maximum river discharge at downstream control point ($m^3\ s^{-1}$), and H_{target} is the defined target reservoir water level (m). All of the $f_{fc,r}$, $f_{fc,d}$ and f_{wu} are between 0 and 1. These three objectives are then formed the objective function f_{obj} through the aggregation approach [*Khu and Madsen*, 2005; *Ngo et al.*, 2007].

$$f_{\mathrm{obj}} = f_{fc,r} + f_{fc,d} + f_{wu}, \quad (14)$$

2.4.2. Constraints

[20] The constraints include mass balance, dam release bounds and storage bounds in the DRESS module [*Saavedra Valeriano et al.* 2010a, 2010b]. In the EPROS, the constraint for release amplitude is also included since dramatic changes in reservoir release may cause damages to the

downstream channels and turbine [*Labadie*, 2004]. In DRESS, the upper and lower boundaries of release are the mean plus and minus one standard deviation, respectively [see *Saavedra Valeriano et al.*, 2010a]. In EPROS, the reservoir release ability (related to reservoir water level) and downstream water requirements (determined by flood control standard and ecological water requirements) are considered.

2.4.2.1. Mass Balance Equation

[21] The mass balance equation is

$$V_{i+1} = V_i + (Qin_i - Qout_i - Qloss_i)\Delta t, \tag{15}$$

where V_i and V_{i+1} are initial and final reservoir storage volumes during time period i, (m^3), Qin_i and $Qout_i$ are reservoir inflow and outflow ($m^3\ s^{-1}$), $Qloss_i$ is the reservoir water leakage ($m^3\ s^{-1}$), and Δt is the reservoir operation time interval (s).

2.4.2.2. Release Bounds

[22] The release bounds are described as

$$Q_{i,\min} \le Qout_i \le Q_{i,\max}, \tag{16}$$

where $Q_{i,\min}$ and $Q_{i,\max}$ are minimum and maximum reservoir release ($m^3\ s^{-1}$). The $Q_{i,\min}$ is constrained by the minimum water demand. The $Q_{i,\max}$ is constrained by reservoir release ability and flood control requirement at control point,

$$Q_{i,\max} = \min\{Q_{i,\text{ability}}, Qctl_{i,\max} - Qinc_i\}, \tag{17}$$

where $Q_{i,\text{ability}}$ is the reservoir release ability ($m^3\ s^{-1}$) and $Qinc_i$ is the interval coming water amount ($m^3\ s^{-1}$).

2.4.2.3. Release Amplitude

[23] The release amplitude is

$$|Qout_i - Qout_{i-1}| \le \Delta Q, \tag{18}$$

where ΔQ is the variation amplitude constraint between period $i-1$ and period i ($1 < i \le T$; $m^3\ s^{-1}$).

2.4.2.4. Storage Bounds

[24] The storage bounds are

$$V_{\text{dead}} \le V_i \le V_{\text{lmt}}, \tag{19}$$

where V_{dead} and V_{lmt} are the water volumes corresponding to dead water level and limited water level (m^3).

2.4.3. Constraints Handling

[25] The constraints are treated simply in DRESS by defining reservoir operation rules artificially [*Saavedra Valeriano et al.*, 2010a, 2010b]. In EPROS, the constraint problem is converted to nonconstraint problem through the widely used penalty function approach [*Yeniay*, 2005; *Michalewicz*, 1995]. The penalty functions measure the violation of the constraints (or penalize unfeasible solutions). The dynamic penalty approach where the penalty value is dynamically modified is superior to stationary penalty approach [*Yeniay*, 2005; *Barakat and Ibrahim*, 2011]. A dynamic penalty function [*Yeniay*, 2005] is defined as

$$H_j = (Ck)^{\alpha}(f_j)^{\beta}, \quad 1 \le j \le p, \tag{20}$$

where C, α, and β are constants, and $C = 1$, $\alpha = 0.5$, $\beta = 2$ in this study; k is the algorithm's current iteration number; f_j ($1 \le j \le p$) is defined from the constraints (equations (16)–(19)) and p ($p = 5$ in this study) is the total number of f_i:

$$f_1 = \sum_{i=1}^{T}\left[\min\left(0, Qout_i - Q_{i,\min}\right)^2\right], \tag{21}$$

$$f_2 = \sum_{i=1}^{T}\left[\max\left(0, Qout_i - Q_{i,\max}\right)^2\right], \tag{22}$$

$$f_3 = \sum_{i=2}^{T}\left[\max(0, |Qout_i - Qout_{i-1}| - \Delta Q)^2\right], \tag{23}$$

$$f_4 = \sum_{i=1}^{T}\left[\min\left(0, V_i - V_{i,\min}\right)^2\right], \tag{24}$$

$$f_5 = \sum_{i=1}^{T}\left[\max\left(0, V_i - V_{i,\max}\right)^2\right], \tag{25}$$

[26] The penalty function is nonzero (greater than 0) when the constraint is violated, and it is zero in the region where constraint is not violated [*Yeniay*, 2005]. By adding the penalty function (equation (20)) to the objective function (equation (14)), the constraint problem is transformed to nonconstraint problem,

$$F = f_{\text{obj}} + \min\left(\sum_{j=1}^{p} H_j\right), \tag{26}$$

[27] If the constraint is violated, equation (26) will be added by a big term (ΣH_j, $1 \le j \le p$), which means the solution is not feasible. In this case, the iterations will repeat and the solution is pushed back toward the feasible region [*Yeniay*, 2005] until the optimal value is found. The feasible solutions should have F between 0 and 3. The lower the F is, the better the solution is. The state variable is V_i and the decision variable is $Qout_i$.

2.4.4. Optimization Scheme

[28] The shuffled complex evolution method developed at the University of Arizona (SCE-UA) [*Duan et al.*, 1992, 1993, 1994] is used in this study. SCE-UA is a robust and effective global optimization strategy and based on a synthesis of controlled random search, competitive evolution and complex shuffling [*Duan et al.*, 1992]. The SCE-UA algorithm has been widely applied for hydrological model parameters calibration [e.g., *Sorooshian et al.*, 1993; *Boyle et al.*, 2000; *Vrugt et al.*, 2003; *Chu et al.*, 2010] and reservoir optimization [e.g., *Ngo et al.*, 2007; *Saavedra Valeriano et al.*, 2010a, 2010b].

[29] A brief description of the method is given below and detailed explanations of the method are given by *Duan et al.* [1992, 1993, 1994]. First, a "population" of points is randomly generated from feasible parameter space; second, the population is partitioned into several complexes; third, each complex is made to evolve in order to direct the search in an improvement direction; fourth, the entire

population is shuffled and points are reassigned to complexes periodically so as to share the information gained by each community. The above evolution and shuffling steps are repeated until termination criteria are satisfied [*Sorooshian et al.*, 1993].

[30] The dam operation time step is 24 h (daily) and the lead time is 192 h (8 days). They are defined according to the NWP product (section 3.2). The WEB-DHM running time step is 1 h.

3. Data Sets

3.1. Study Region and Reservoir Characteristics

[31] The Fengman basin locates at the upper reach of the Second Songhua River in Northeast part of China (Figure 2a), and has a catchment area of 42,500 km^2. The Hongshi-Fengman subbasin which has abundant rain gauges (data set introduced in section 3.3.1) is 22,600 km^2 (white in Figure 2b). The Fengman reservoir was built in 1937 and begun to store water in 1942. The reservoir's target mainly includes flood control and hydropower generation. The capacity of the reservoir is 10,988 million m^3. The annual runoff distributed unevenly with 70% inflow concentrating in flood season from June to September. The annual mean runoff is also nonuniform with maximum and minimum values equal 737 and 164 m^3 s^{-1}, respectively. This basin is characterized by temperate semiarid continental climate. The average annual precipitation is approximately 700 mm with 60%–90% precipitation concentrated in flood season (from June to September). The large amount rainfall often occurs in a short period of time, and they are usually violent and cover large areas [*Asian Development Bank*, 2002]. This area also subjects to long-term water shortage in nonflood seasons particularly in spring. Furthermore, the downstream Jilin and Harbin city are important cities for protection. Therefore, the proper operation of Fengman reservoir is essential to this region. The reservoir associate parameters are summarized in Table 1. Other parameters include reservoir storage-capacity curve, discharging curve, and characteristic water level (not shown).

3.2. Numerical Weather Predictions

[32] The deterministic NWP data were obtained from the Global Spectral Model (GSM) of Japan Meteorological Agency (JMA). GSM provides deterministic NWP products four times a day with 84 h forecasts from 00:00, 06:00 and 18:00 UTC and 192 h forecasts from 12:00 UTC (coordinated universal time). A more detailed description of JMA's NWP is given by *Saito et al.* [2007], *Yamaguchi et al.* [2009], and *JMA* [2007].

[33] The available meteorological parameters for JMA's deterministic NWP products include winds (zonal and meridional), air temperature, relative humidity, surface pressure, total precipitation or rain. The forecast lead time is 192 h and the initial time is 12 UTC. The temporal resolution is 6 h within 96 h forecast and it is 12 h for a 96–192 h forecast. The spatial resolution is 1.25°.

[34] The JMA's operational Ensemble Prediction System (EPS) for weekly forecasting runs up to 9 days once a day at 12:00 UTC [*JMA*, 2007]. The ensemble size of 1 week EPS is 25 until March 2006, while it is 51 after that. The temporal resolution is 24 h. The spatial resolution is 1.875°

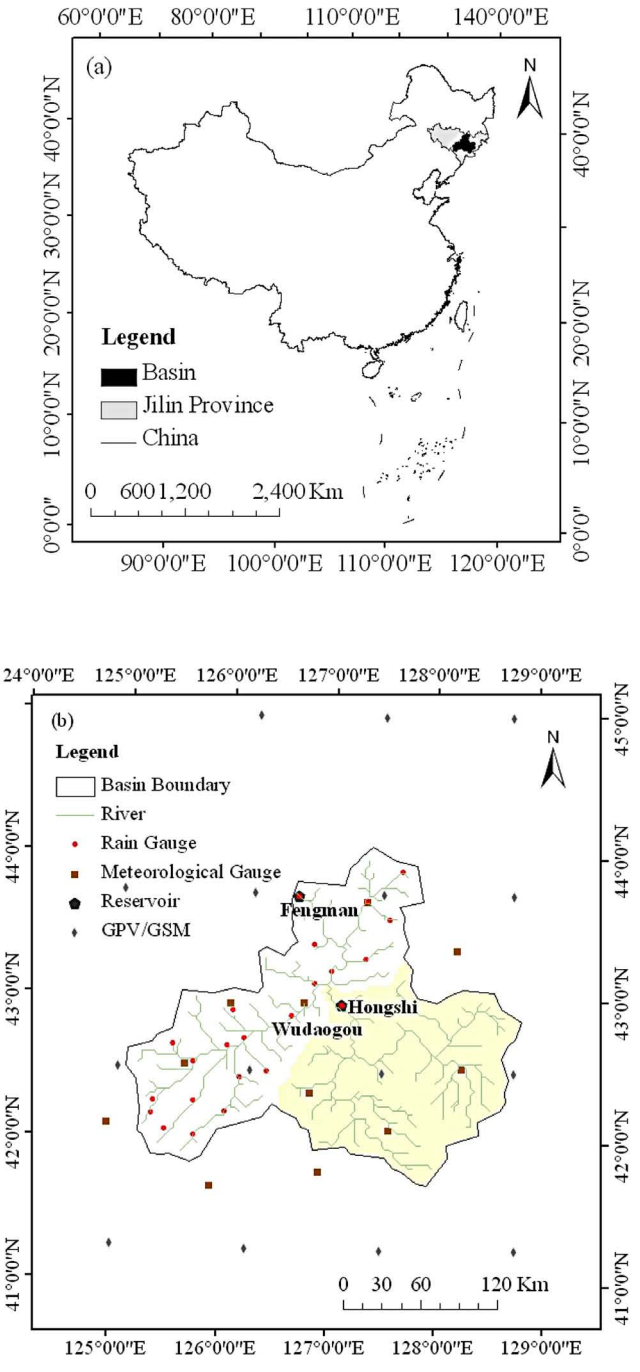

Figure 2. The Fengman basin: (a) the location in China and (b) the basic hydrometeorological data sets.

for Asian area, and it is 2.5° for global. The JMA's ensemble QPFs are used in this work. Both of the deterministic and ensemble NWP products are available from 15 May 2002 and they can download from http://gpvjma.ccs.hpcc.jp/~gpvjma/ and http://database.rish.kyoto-u.ac.jp/arch/jmadata/data/gpv/original/.

3.3. Ground-Based Observations

3.3.1. Atmospheric Forcing Data

[35] The ground-based meteorological observations include daily precipitation, relative humidity, wind speed,

Table 1. Fengman Reservoir Characteristic Parameters

Parameters	Value
Dead water level H_{dead}	242.00 m
Limited water level H_{lmt}	257.90–263.50 m
Dead water volume V_{dead}	26.85×10^8 m^3
Water volume corresponding to limited water level V_{lmt}	88.49×10^8 m^3
Minimum river discharge at control point $Qctl_{min}$	218 m^3 s^{-1}
Maximum river discharge at control point $Qctl_{max}$	2500 m^3 s^{-1}
Variation amplitude constraint between periods $i-1$ and i (ΔQ)	600 m^3 s^{-1}

daily maximum temperature, daily minimum temperature, daily average temperature and sunshine duration. There are 23 rain gauges in the basin (Figure 2b) and hourly precipitation data were downscaled from daily rain gauge observation data using a stochastic method [*Yang et al.*, 2004b]. Data from 11 meteorological sites (Figure 2b) were taken. Hourly temperatures were calculated from daily maximum and minimum temperatures using the TEMP model [*Parton and Logan*, 1981]. Downward shortwave radiation was estimated from sunshine duration, temperature, and humidity using a hybrid model developed by *Yang et al.* [2001, 2006]. Downward longwave radiation was estimated from temperature, relative humidity, pressure, and solar radiation using the relationship between shortwave radiation and longwave radiation [*Crawford and Duchon*, 1999]. Air pressure was estimated according to the altitude [*Yang et al.*, 2006]. These meteorological data were then interpolated to 3000 m model cells through inverse distance weighting (IDW) method. The surface air temperature inputs were further modified with a lapse rate of 6.5 K km^{-1} considering the elevation differences between the model cells and meteorological stations.

3.3.2. Model Evaluation Data

[36] The observed daily inflows for Fengman reservoir (Figure 2b) from 2000 to 2005 are used to evaluate the WEB-DHM model. The observed reservoir status data were used to examine the performance of dam operation system. These reservoir status data include daily inflow, release, water level (storage), as well as water loss data. The flood events of 2001 (25 July to 25 August), 2004 (17 July to 15 August) and 2005 (8 to 27 August) are taken in this research because of their high flood peaks. They are once-in-a-decade floods with the peak inflows of Fengman reservoir are 5328, 3242, and 3429 m^3 s^{-1} for 2001, 2004, and 2005 flood events.

3.4. Satellite Data

[37] DEM data were obtained from the United States Geological Survey (USGS) Seamless Data Distribution System (http://seamless.usgs.gov/) and the subgrid topography was described by a 100 m DEM. The elevation of the basin varies from 168 to 2396 m (Figure 3a) and the grid slopes vary from 0° to 27° (Figure 3b). Land use data were obtained from the USGS (http://edc2.usgs.gov/glcc/glcc.php). The land use types have been reclassified to SiB2 land use types for the study [*Sellers et al.*, 1996a]. There are 8 land use types, with broadleaf and needleleaf trees being the main type (Figure 3c). Soil data were obtained from the *Food and Agriculture Organization* [2003] global data product. There are 6 kinds of soil in the basin, with sandy clay loam-lithosols (I-Bk) being the dominant type (Figure 3d).

[38] Static vegetation parameters include morphological, optical and physiological properties defined by *Sellers et al.* [1996b]. Dynamic vegetation parameters including the leaf area index (LAI) and the fraction of photosynthetically active radiation (FPAR) absorbed by the green vegetation canopy were obtained from the MOD15A2 1 km 8 day products [*Myneni et al.*, 1997]. They were downloaded through the Warehouse Inventory Search Tool (WIST, https://wist.echo.nasa.gov/~wist/api/imswelcome/).

3.5. Reanalysis Product

[39] The interim reanalysis produced by European Center for Medium-Range Weather Forecasts (ERA-Interim [*Dee et al.*, 2011]) is used as EPROS forcing data for 2001 since the JMA's NWP data (see section 3.2) are not available. The temporal and spatial resolutions for ERA-Interim forecast data are 3 h and 0.703125° (N128 reduced Gaussian grid), respectively. ERA-Interim covers the period from 1 January 1979 onward, and continuing in near-real time. The detailed descriptions for ERA-Interim can be found at http://www.ecmwf.int/research/era/.

4. Results

4.1. WEB-DHM Evaluation

[40] The WEB-DHM has been carefully calibrated and evaluated with daily discharges and 8 day land surface temperatures in the upper reach of the Wudaogou subbasin (Figure 2b) from 2000 to 2006 [see *Wang et al.*, 2011]. It should be noted that the real-time EPROS system is expected to be fed with atmospheric parameters. In this study, the rainfall observations at the upper reach of the Hongshi reservoir are not available. In addition, this work mainly aims to demonstrate singe-reservoir (Fengman reservoir) real-time optimization method. Therefore, the observed outflows of Hongshi (Figure 2b) reservoir are embedded into the WEB-DHM. The following statistical variables are used to evaluate the performances of the WEB-DHM:

$$\mathrm{NS} = 1 - \sum_{i=1}^{n} (X_{oi} - X_{si})^2 \Big/ \sum_{i=1}^{n} (X_{oi} - \overline{X}_0)^2, \tag{27}$$

$$\mathrm{BIAS} = \left(\sum_{i=1}^{n} X_{si} - \sum_{i=1}^{n} X_{oi} \right) \Big/ \left(\sum_{i=1}^{n} X_{oi} \right) \times 100\%, \tag{28}$$

where X_{oi} is the observed value, X_{si} is the simulated value, n is the total number of time series for comparison, and $\overline{X}_0$ is the mean value of X_{oi} over the comparison period. The higher NS is, the better the model performs. A perfect fit should have a NS value equal to one [*Nash and Sutcliffe*, 1970]. The lower BIAS is, the better the model performs. A perfect fit should have BIAS equal to zero.

[41] Figure 4 shows the daily discharge (Q) at Fengman reservoir simulated by the WEB-DHM. Figure 4a reveals the discharges are well reproduced from 2000 to 2005 with NS equal to 0.843 and BIAS equal to 12.29%. The simulated discharges during flood seasons in 2001 (from 25 July to

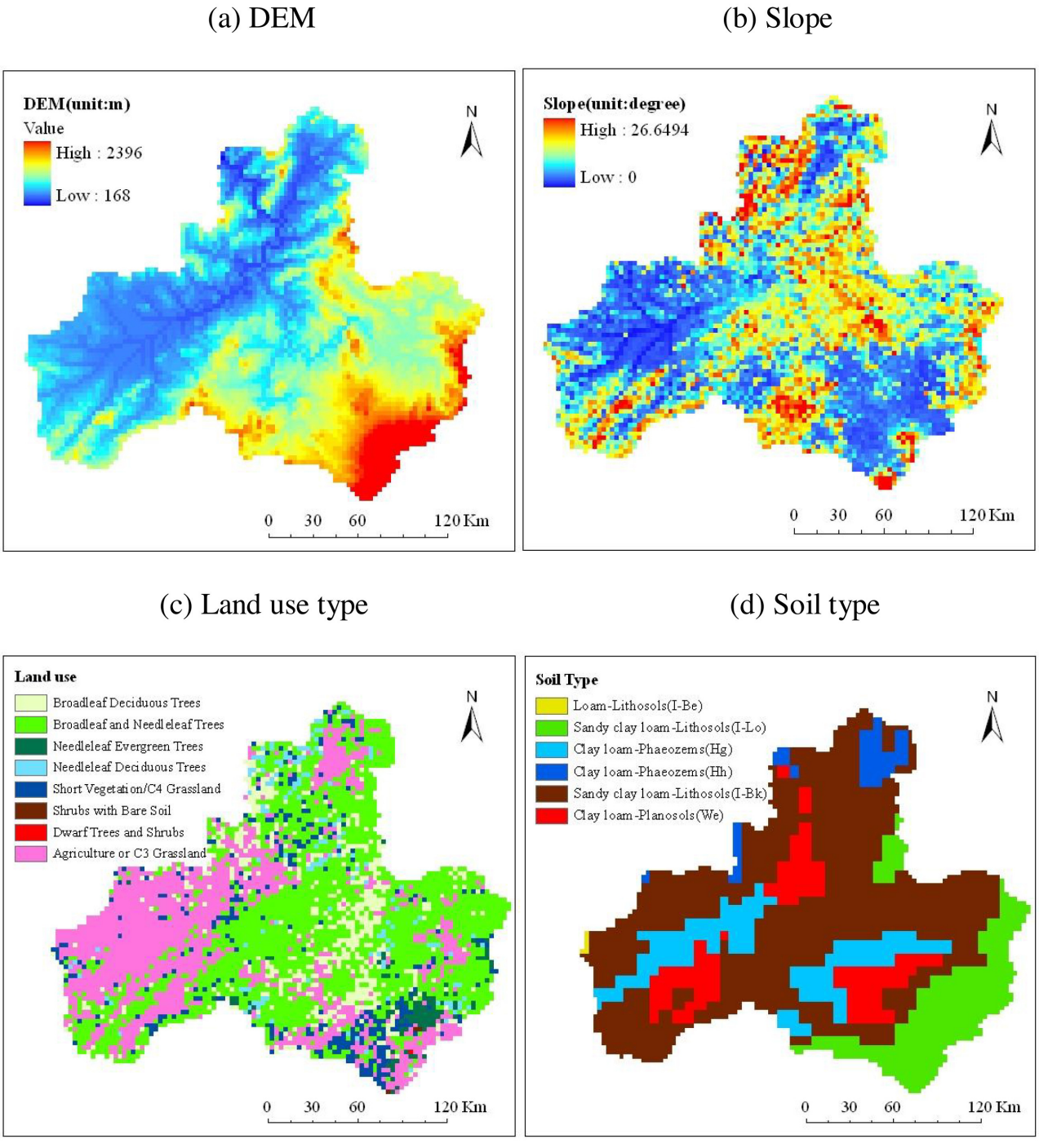

Figure 3. (a) The digital elevation model (DEM), (b) grid slope, (c) land use, and (d) soil type used by WEB-DHM.

25 August, Figure 4b), 2004 (from 17 July to 15 August, Figure 4c) and 2005 (from 8 to 27 August, Figure 4d) show the NS is larger than 0.931 and BIAS (absolute value) is smaller than 4.39%. It is possible that the observed outflows of Hongshi reservoir have influences on the high NS value. However, the Fengman reservoir is the target reservoir in this work. The observed discharges at Hongshi reservoir are used. These evaluation results indicate the WEB-DHM is able to predict river discharge (especially during flood seasons) reasonably well. Therefore, the WEB-DHM is then applied to predict Fengman reservoir inflows during flood seasons.

4.2. QPF Perturbation and Evaluation

4.2.1. Deterministic QPF Evaluation

[42] Four rainfall events selected from the 2004 and 2005 flood seasons are evaluated because of their high rainfall intensities and the available data sets for both

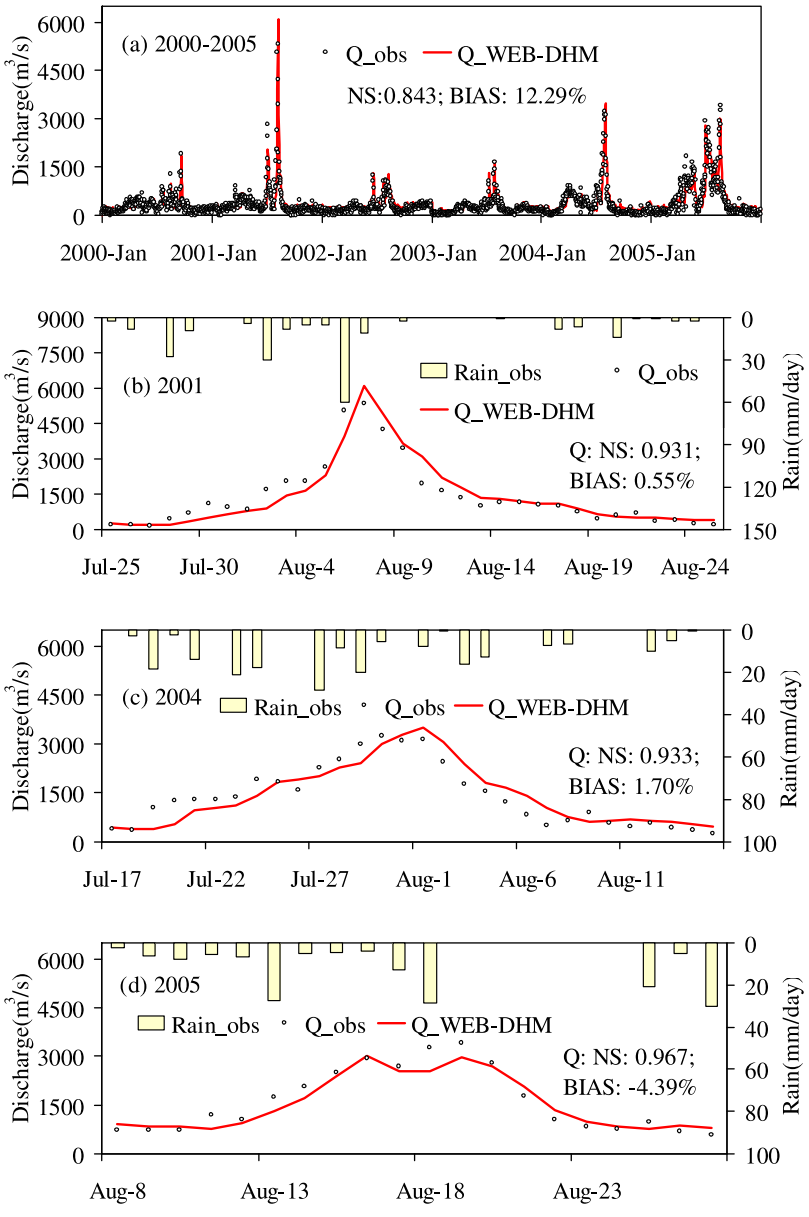

Figure 4. (a) The Fengman dam daily inflows simulated by the WEB-DHM and the enlarged hydrograph for (b) the 2001 flood season (25 July to 25 August), (c) 2004 flood season (17 July to 15 August), and (d) 2005 flood season (8–27 August).

observations and forecasts. The maximum and basin average (Hongshi-Fengman basin) rainfall intensities are 75.3 mm d^{-1} and 41.0 mm d^{-1} for 23 July 2004, 57.6 mm d^{-1} and 26.7 mm d^{-1} for 29 July 2004, 104.7 mm d^{-1} and 35.5 mm d^{-1} for 12 August 2005, and 72.4 mm d^{-1} and 39.1 mm d^{-1} for 17 August 2005. The following statistical variables are used to evaluate the performances of the deterministic QPF:

$$\mathrm{MBE} = \left(\sum_{i=1}^{n} X_{si} - \sum_{i=1}^{n} X_{oi}\right)/n \times 100\%, \tag{29}$$

$$\mathrm{RMSE} = \left[\frac{1}{n} \times \sum_{i=1}^{n} (X_{si} - X_{oi})^2\right]^{\frac{1}{2}}, \tag{30}$$

[43] The lower MBE or RMSE is, the better the model performs. A perfect fit should have MBE or RMSE equal to zero.

[44] Figure 5 compares the spatial distribution of daily accumulated precipitation between observations and JMA's deterministic NWP with different lead time (1 day, 2 days, 3 days, 5 days and 8 days) on 23 July 2004 (Figure 5a), 29 July 2004 (Figure 5b), 12 August 2005 (Figure 5c) and 17 August 2005 (Figure 5d). In general, the QPFs show both intensity error (e_{itn}) and distribution error (e_{dis}). The precipitation intensities of observations (1st row of Figure 5) show larger values than the deterministic QPFs forecasts. The spatial distributions of JMA's deterministic forecasts are more uniform than observations because of the lower spatial resolution of the JMA NWP points (1.25°) comparing with rain gauges (around 0.25° to 0.30°). The maximum precipitation center locates at the southwest part of the basin for all the observations, while it locates at western part of the region for most JMA NWP forecasts.

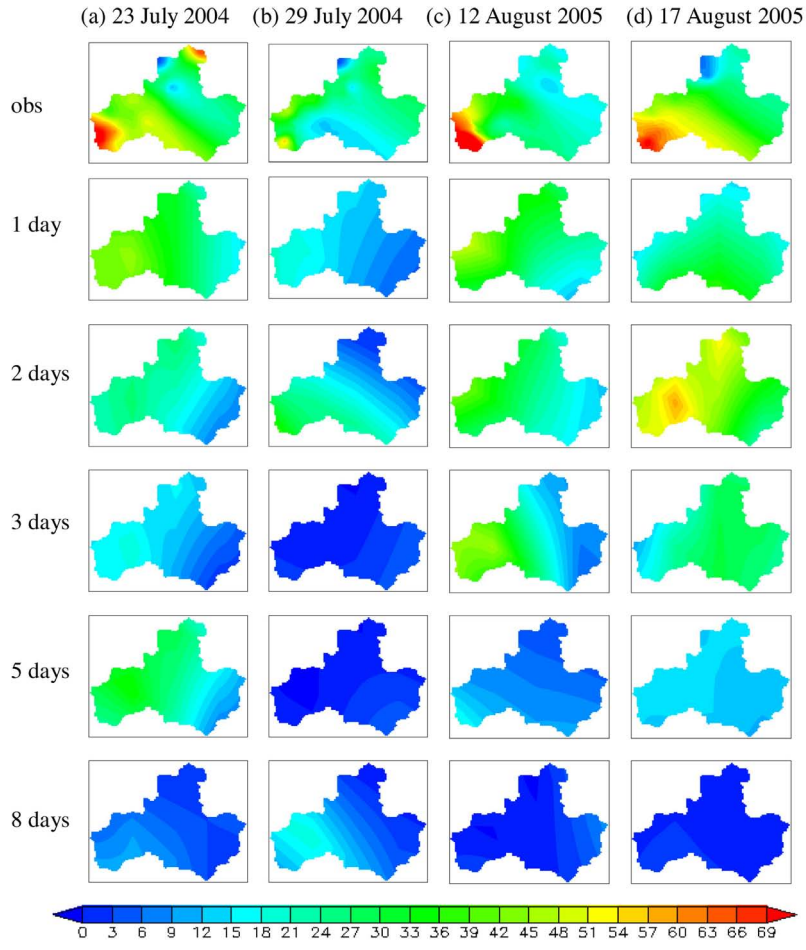

Figure 5. The spatial distribution of the daily accumulated precipitation (APCP; in mm) for the observation (first row) and the Japan Meteorological Agency (JMA) deterministic numerical weather predictions (NWP) with lead times of 1, 2, 3, 5, and 8 days (second to sixth rows) on (a) 23 July 2004, (b) 29 July 2004, (c) 12 August 2005, and (d) 17 August 2005.

[45] Figure 6 shows the variation of maximum and basin average (Hongshi-Fengman basin) precipitation intensities with different lead time between JMA's deterministic NWP and observations on 23 July 2004 (Figures 6a and 6b), 29 July 2004 (Figures 6c and 6d), 12 August 2005 (Figures 6e and 6f) and 17 August 2005 (Figures 6g and 6h). The maximum (dashed lines in Figures 6a, 6c, 6e, and 6g) and mean (dashed lines in Figures 6b, 6d, 6f, and 6h) intensities for the deterministic QPFs are lower than observations (solid lines in Figure 6) for most events. In general, the accuracy of QPF predictions decreases with the lead time increasing from 1 day to 8 days.

[46] Figure 7 shows the variation of MBE and RMSE for JMA NWP maximum and basin average (Hongshi-Fengman basin) precipitations (deterministic forecast) with different lead time from 17 July to 15 August 2004 (Figures 7a and 7b) and from 8 to 27 August 2005 (Figures 7c and 7d). The MBE (absolute value) and RMSE increase with the lead time increasing from 1 day to 8 days for all the events. The forecast basin average precipitation performs better than maximum precipitation. The absolute value of MBE (RMSE) for 2004 QPF (Figures 7a and 7b) increases from 6.46 mm d^{-1} (19.22 mm d^{-1}) to 14.80 mm d^{-1} (26.55 mm d^{-1}) and from 1.98 mm d^{-1} (7.52 mm d^{-1}) to 4.64 mm d^{-1} (10.94 mm d^{-1}) with the lead time increasing from 1 to 8 days for maximum precipitation and mean precipitation, respectively. The QPF in 2005 shows the same trend with the QPF in 2004. Many studies depicted that the NWP forecast skill is decreased as a function of forecast lead time [e.g., *Lin et al.*, 2005]. The uncertainty in atmosphere states and the complexity of the atmospheric equations limit the forecast model accuracy to about 5 or 6 days [*Chakraborty*, 2010].

[47] In summary, the JMA's deterministic NWP makes sense on precipitation forecasting but there are biases for rainfall intensities and spatial distributions especially for the lead time longer than 5 days. Therefore, the further processing (e.g., perturbation) of rough deterministic QPF is necessary before practical applications.

4.2.2. QPF Perturbation

[48] The deterministic QPFs for 2004 and 2005 are perturbed through equation 7. The perturbation contains 30 members for illustration and the further discussions on ensemble size are elaborated in section 5.1. Figure 8 shows the deterministic and perturbed QPFs (1 day lead time) comparing with observations averaged at the Hongshi-Fengman

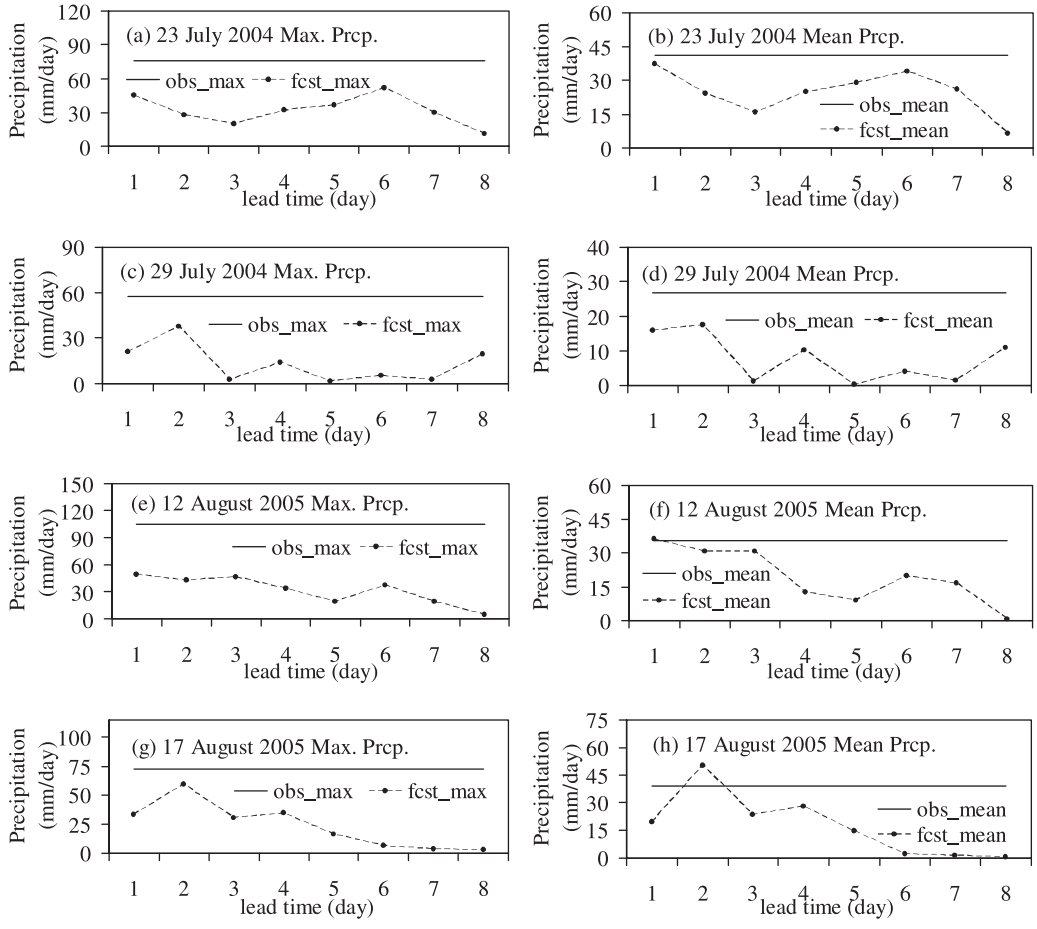

Figure 6. The maximum and basin average (Hongshi-Fengman basin) precipitation intensities for the observation and the JMA deterministic NWP with different lead times on (a, b) 23 July 2004, (c, d) 29 July 2004, (e, f) 12 August 2005, and (g, h) 17 August 2005.

basin from 17 July to 15 August 2004 (Figure 8a) and from 8 to 27 August 2005 (Figure 8b). The JMA's deterministic NWP successfully captures the major rainfall events (e.g., 23 and 29 July 2004, 3 and 7 August 2004, 12 and 17 August 2005), but the amount of maximum precipitation is higher or lower than observed values. The observed and forecast values of the maximum precipitation on 3 August 2004 are 19.4 and 32.1 mm d^{-1}, respectively. The perturbed forecast values are between 6.3 and 50.7 mm d^{-1} (values not shown). The perturbed forecast captures the observed sceneries correctly. The other rainfall events also demonstrate the discrepancies between JMA NWP deterministic forecast and

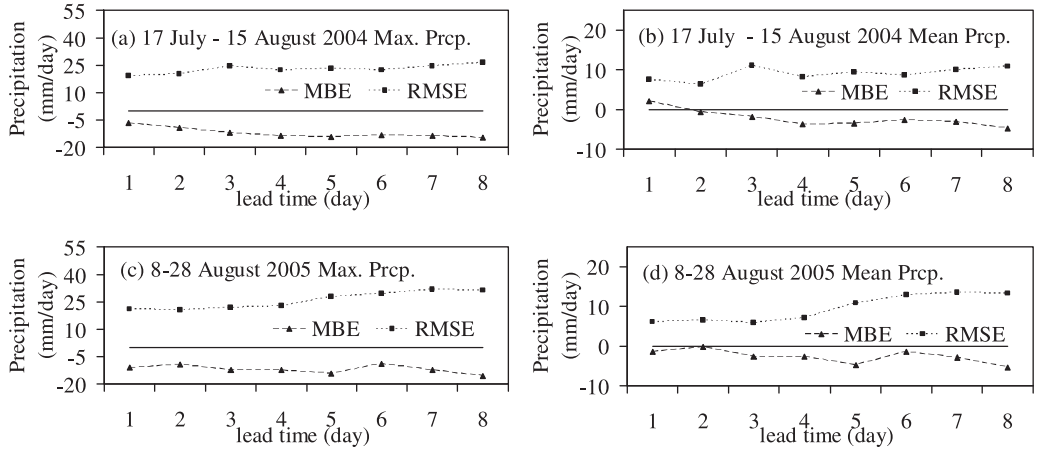

Figure 7. The MBE and RMSE of maximum and basin average (Hongshi-Fengman basin) precipitation intensities for the JMA deterministic NWP with different lead times.

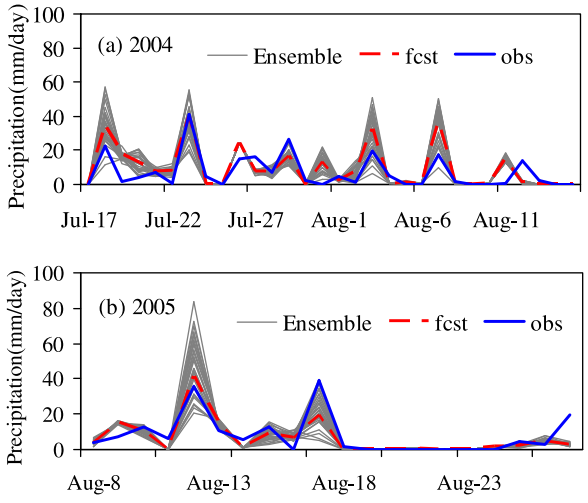

Figure 8. The daily precipitation of JMA deterministic NWP forecasts and the perturbed forecasts (both with 1 day lead time) compared to the observations averaged at the Hongshi-Fengman basin (except the Hongshi subbasin): (a) from 17 July to 15 August 2004 and (b) from 8 to 27 August 2005. Here the ensemble uses 30 members; fcst and obs refer to forecast and observation, respectively.

observed values are dampened by the perturbed forecasts through generating a variety of sceneries.

4.2.3. Probabilistic QPF Evaluation

[49] The continuous ranked probability score (CRPS) [*Hersbach*, 2000] and rank histogram (RH) [*Hamill*, 2001] are used to evaluate the performance of probabilistic QPF. The CRPS calculates the difference between the predicted and the observed cumulative density functions (CDFs) of variables [*Candille et al.*, 2007]. The lower CRPS is, the better the prediction performs. The RH checks the probability of the verifying observations falling between any two adjacent members of the ensemble forecast data [*Pappenberger et al.*, 2009]. A perfect ensemble spread shows a flat RH because each member represents an equally scenario [*Hamill*, 2001].

[50] In this section, an additional 25-member ensemble QPFs are generated by EPROS in order to keep consistence with JMA 25-member ensemble NWPs. Figures 9a and 9b compare the CRPS for ensemble QPFs obtained from JMA and EPROS during the flood seasons of 2004 and 2005. The mean CRPS of QPFs equals 3.8 and 4.1 for JMA and EPROS in 2004, while they are 5.1 and 3.7 in 2005. Averaged for 2004 and 2005, the CRPS of QPFs is 4.3 and 4.0 for JMA and EPROS, respectively. In general, the EPROS performed better than JMA in generating ensemble QPFs for these particular cases. The difference in the CRPS is significant at 0.05 ($\alpha = 0.05$) significance level by using F test ($F = 2.68 > F_{0.025,50,50} \approx 1.7$). The main reason is the nature of ensemble generation is different. For JMA, the initial conditions are integrated by using a low-resolution version of JMA global spectral model (GSM) for producing an ensemble of 9 day forecasts in the 1 week EPS. The perturbed initial fields are obtained using the Breeding of Growing Modes (BGM) method [*JMA*, 2007]. However, EPROS use a kind of statistical generation depending on the error analysis using past observations.

[51] Figures 9c and 9d draw the RH for ensemble QPFs obtained from JMA and EPROS calculated from the flood seasons of 2004 and 2005. Both of the JMA and EPROS ensemble QPFs show U-shaped RH. This result indicates that many observations falling outside of the ensemble boundaries. The RH of the two ensembles performed similarly with the frequency of observations falling outside of ensemble extremes is 0.63 and 0.65 for JMA and EPROS, respectively.

4.3. Reservoir Optimization

[52] The EPROS system is examined on Fengman reservoir for 2004 and 2005 flood events. The Hongshi reservoir (see Figure 2b) releases are embedded into the hydrological model (WEB-DHM). The Fengman reservoir outlet is used as the control point because of the available observations. In this case, the discharges at the control point ($Qctl_i$) equal to the Fengman reservoir release ($Qout_i$). The initial reservoir water levels are set as 253.67 and 257.58 m (observed values) for 2004 and 2005 flood events, respectively. In this

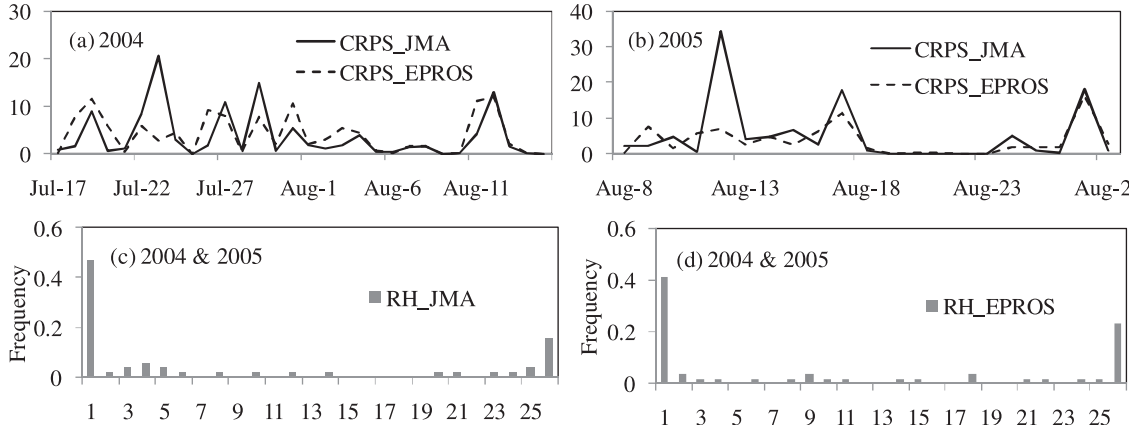

Figure 9. Comparison of continuous ranked probability score (CRPS) and rank histogram (RH) for ensemble quantitative precipitation forecasts (QPFs) obtained from EPROS and JMA: (a) CRPS from 17 July to 15 August 2004, (b) CRPS from 8 to 27 August 2005, and (c) RH for JMA QPFs and (d) RH for EPROS QPFs from 17 July to 15 August 2004 and from 8 to 27 August 2005.

section, the target water levels are set as 263.50 m (upper bound of limited water level) for both events. The WEB-DHM initial conditions of reservoir operation for 2004 (17 July to 15 August) and 2005 (8–27 August 2005) flood events were obtained by running the model from 1 January 2004 to 16 July 2004 and from 1 January 2005 to 7 August 2005, respectively.

4.3.1. Control Run

[53] Figures 10a and 10b compare the simulated Fengman reservoir releases and water levels with observed values for 2004 and 2005 flood events. The simulated release peak are 748 and 493 $m^3 s^{-1}$ for 2004 and 2005 flood events, respectively. They are much lower than the observed values which are 1952 and 1278 $m^3 s^{-1}$. The simulated maximum amplitude of release variations are 523 and 229 $m^3 s^{-1}$ for 2004 and 2005 flood events. They are also lower than the observed values (555 and 724 $m^3 s^{-1}$). The optimized release with lower variation amplitude is helpful for protecting downstream channels and turbine [*Labadie*, 2004]. The reservoir water levels are 261.63 m and 263.14 m at the end of the flood, while the observations are 257.44 and 262.51 m for 2004 and 2005 flood events. Because the system takes into account the forecast information, the floods are stored in the reservoir during the flood peak and the optimized water levels are higher than the observations at the end of flood events. This is important for reservoir water utilizations (e.g., hydropower generation, agriculture). The optimized maximum reservoir water levels are lower than the upper bound of limited water level (263.50 m) for both flood events. This is important for the reservoir and upstream safety.

[54] Figures 10c and 10d plot the optimized objective functions during the flood events for 2004 and 2005 flood events, respectively. The objective functions are lower than 3.0 for both cases. This result demonstrates the optimized solutions are in feasible space (see 2.4.3).

[55] In summary, JMA's deterministic NWP provides valuable information in guiding real-time reservoir optimization. However, there are uncertainties in forecast reservoir inflows because of the QPF uncertainties. Underestimation of inflow tends to increase water storage but decrease the flood control capacity, while overestimation of inflow is likely to increase flood control ability but decrease the water use efficiency. In fact, the QPF errors are inevitable, especially for the medium- and long-term precipitation forecast, because of the chaotic characters of atmosphere as well as the approximate simulation of atmospheric processes by NWP [*Lorenz*, 1969; *Toth and Kalnay*, 1993; *Buizza et al.*, 2005]. Therefore, it is necessary to take into account the QPF errors for reservoir practical operations.

4.3.2. Ensemble Run

[56] Figure 11 shows the reservoir optimization results through the use of ensemble predictions for 2004 (Figures 11a, 11c, 11e, 11g and 11i) and 2005 (Figures 11b, 11d, 11f, 11h and 11j) flood events. Figures 11a and 11c compare the ensemble reservoir daily inflows (8 day lead time) with the observations and the control run results for 2004 flood event. The predictions are initialized at 18 July 2004 (Figure 11a, flood rising) and 2 August 2004 (Figure 11c, flood recession), respectively. The flood is underestimated for control run (e.g., 20 and 21 July 2004) during flood rising, while it is overestimated during flood recession (e.g., 6 and 7 August 2004). The ensemble floods dampen these uncertainties for most cases. The flood peaks are also well predicted by using ensemble technique for 2005 flood events (see Figures 11b and 11d).

[57] Figure 12 shows the CRPS and RH of ensemble reservoir inflows generated by EPROS for 2004 and 2005 flood events. The CRPS of reservoir inflows varies from 1.6 to 639.0 during flood rising, and from 44.0 to 517.2 during flood recession for 2004 flood event (Figures 12a and

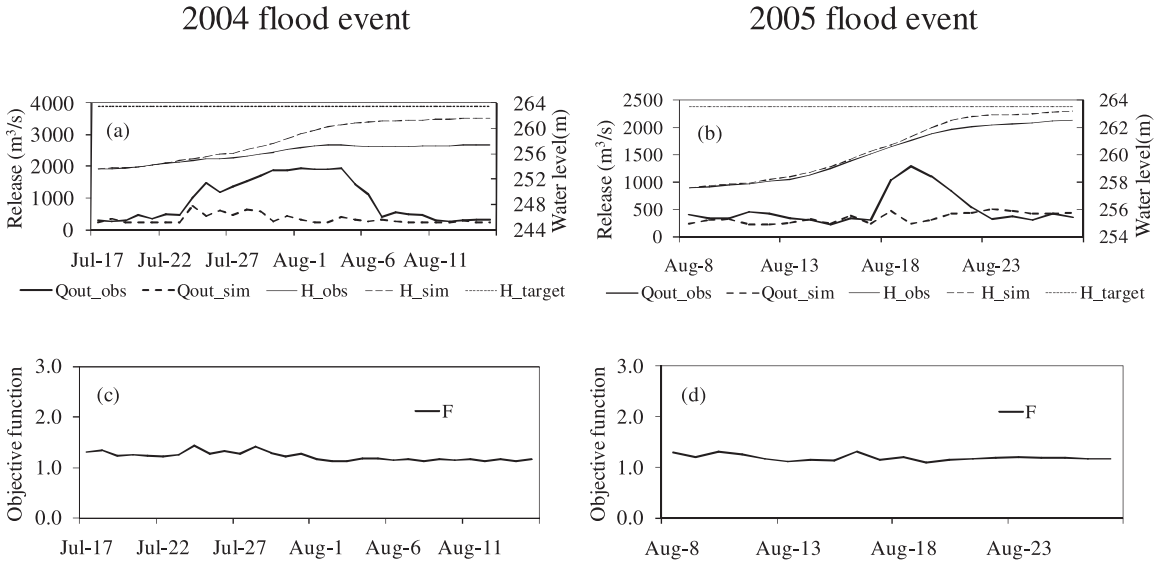

Figure 10. The Fengman reservoir optimization results (daily) using JMA deterministic NWP data from 17 July to 15 August 2004 (Figures 10a and 10c) and from 8 to 27 August 2005 (Figures 10b and 10d): (a and b) the optimized reservoir water level and release and (c and d) the optimized objective function.

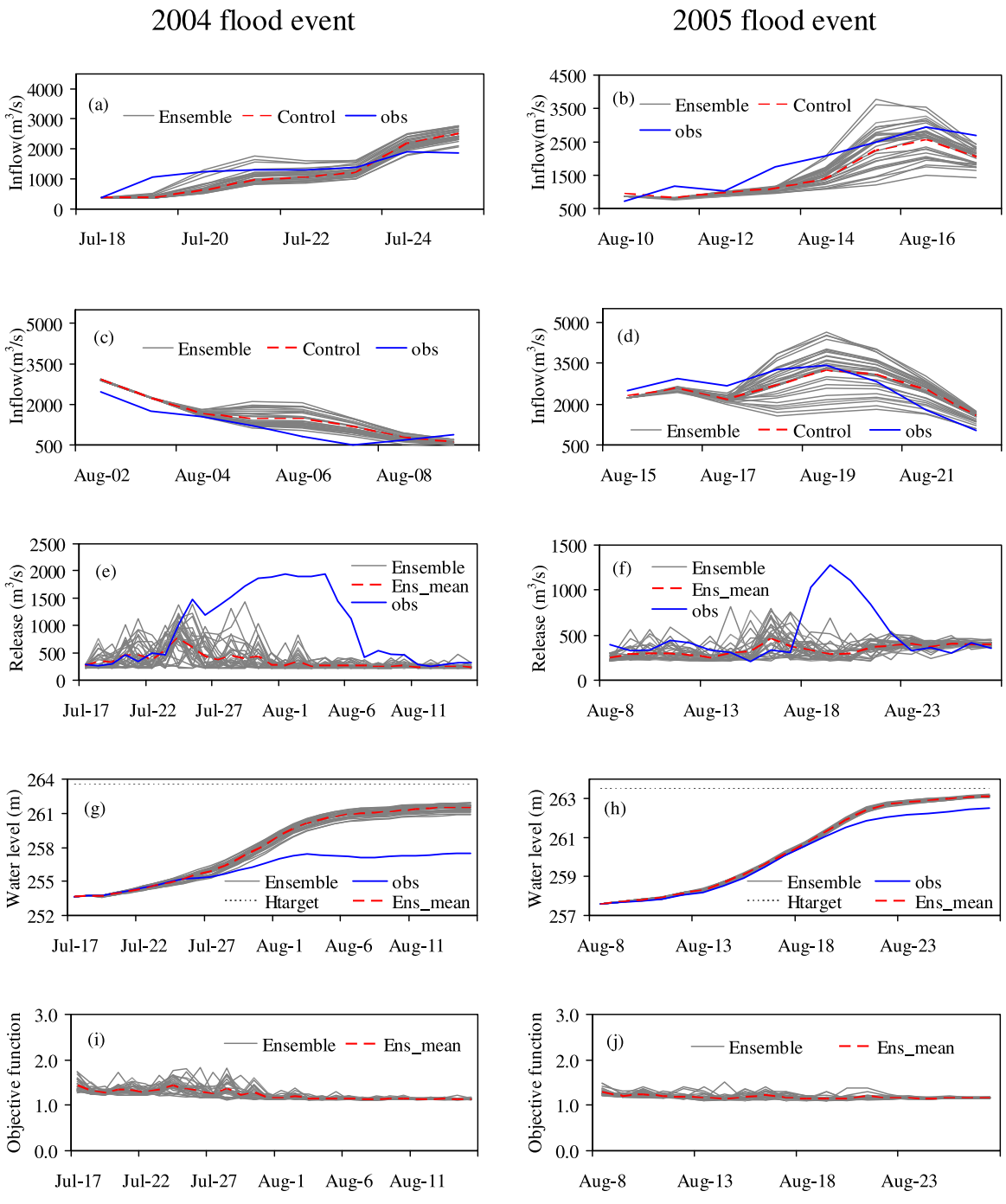

Figure 11. (a–d)The ensemble reservoir daily inflow, (e and f)release, (g and h) water level, and (i and j) objective function for (left) 2004 and (right) 2005 flood events. Here obs refers to observed value, control means the model is fed with deterministic QPF, ens_mean is the ensemble mean value. Here the ensemble uses 30 members.

12c). The CRPS of reservoir inflows is between 82.7 and 639.6 during flood rising, and between 185.8 and 470.4 during flood recession for 2005 flood event (Figures 12b and 12d). Figures 12e and 12f depict the RH for 2004 and 2005 flood events. Both of the 2004 and 2005 flood events show U-shaped RH. The frequency of observations falling outside of ensemble extremes is 0.56 and 0.63 for the 2004 and 2005 flood events, respectively.

[58] Figures 11e and 11f give the ensemble optimized dam releases for 2004 and 2005 flood events, respectively. The peak values of reservoir release of ensemble optimization results and observations are 1430 and 1952 $m^3\ s^{-1}$ for 2004 events, and they are 814 and 1278 $m^3\ s^{-1}$ for 2005 events (Table 2). The ensemble average release peaks are 785 and 462 $m^3\ s^{-1}$ for 2004 and 2005 events. The downstream flood peak is reduced by 59.8% (1167/1952) and

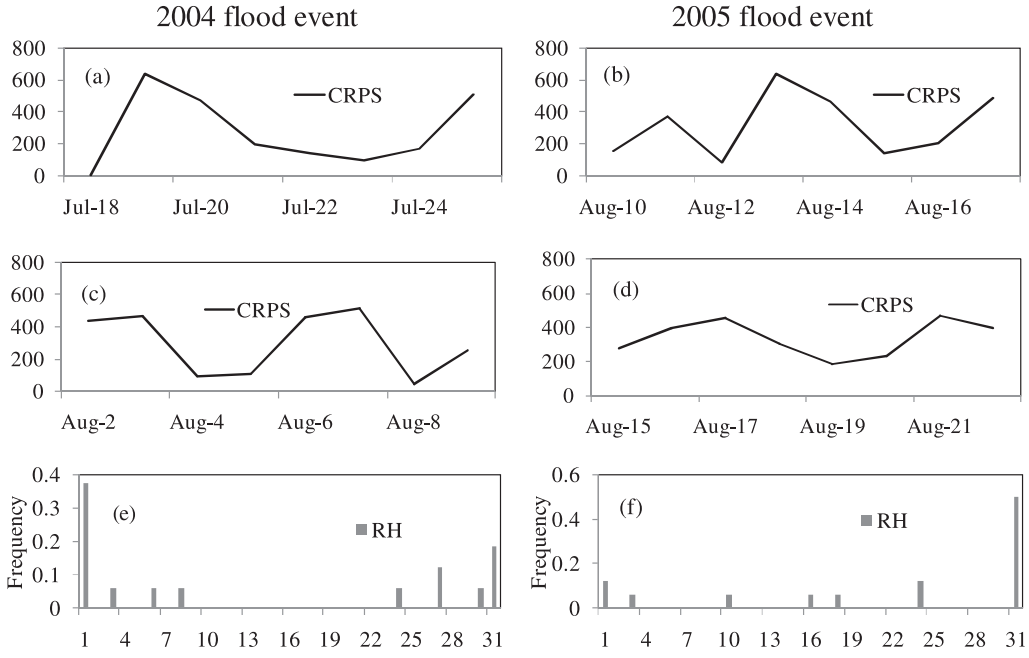

Figure 12. (a–d) The CRPS and (e and f) RH of ensemble reservoir inflows generated by EPROS for (left) 2004 and (right) 2005 flood events.

63.8% (816/1278) for 2004 and 2005 events. The ensemble dam releases provide a reasonable range for the real-time release decision making since the ensemble dam inflows include varies flood sceneries by considering the QPF errors.

[59] Figures 11g and 11h draw the optimized reservoir water levels for 2004 and 2005 flood events, respectively. In Figure 11g, the optimized ensemble end water levels (H_{end}) are between 260.83 m and 261.90 m, and the ensemble average H_{end} is 261.51 m. In Figure 11h, the optimized ensemble end water levels (H_{end}) are between 260.83 m and 261.90 m, and the ensemble average H_{end} is 263.13 m. All of the 30 ensemble dam end water levels are higher than the observed values (257.44 m for 2004 and 262.51 m for 2005), and they are lower than the upper bound of limited water level (263.50 m; see Table 2). The increased water volumes are 8.67×10^8 and 1.69×10^8 m^3 for 2004 and 2005 flood events, respectively. The increased water amount is very important for alleviating long-term water shortage problem for this semiarid region during nonflood seasons particularly in spring. The maximum water levels are decreased by 1.99 and 0.37 m for 2004 and 2005 flood events, respectively (Table 2). This is essential for reservoir and upstream safety.

[60] Figures 11i and 11j illustrate the optimized objective functions for 2004 and 2005 flood events, respectively. All of the objective functions satisfy the constraints with the range between 0.0 and 3.0. These results demonstrate the well performance of the optimization system.

Table 2. Fengman Reservoir Optimization Results (30-Member Ensemble Mean) Compared With Observations

Flood	Maximum Water Level (m)	Downstream Flood Peak ($m^3 s^{-1}$)	End Water Level (m)
2001			
Optimization	261.37	1199	261.36
Observation	263.50[a]	1922	259.26
Benefit	2.13	723	2.10
2004			
Optimization	261.51	785	261.51
Observation	263.50[a]	1952	257.44
Benefit	1.99	1167	4.07
2005			
Optimization	263.13	462	263.13
Observation	263.50[a]	1278	262.51
Benefit	0.37	816	0.62

[a]Upper bound of limited water level, obtained from the Fengman reservoir operation rule.

5. Discussion

5.1. The Sensitivity to Ensemble Size

[61] The proper ensemble size (m) is important for reservoir real-time optimization. The small ensemble size is beneficial for computer storage space and computing time but it may lose flood sceneries. The large ensemble size is expected to generate wider flood ranges, while the computing time is long [*Frogner and Iversen*, 2001]. Therefore, this section investigates the sensitivity to ensemble size for the system optimization by comparing the 10-member and 50-member ensemble streamflows, reservoir releases, water levels and objective functions.

[62] The spread and error diagram, as well as the percentage of outliers (PO) are used to measure the performance of the ensemble forecast with different ensemble size. The PO is classified as the proportion of observations outside the 10% and 90% percentiles of ensemble forecasts [*Pappenberger et al.*, 2009]. The ensemble spread is calculated from the difference between the 90% and 10% percentiles of ensemble forecasts [*Pappenberger et al.*, 2009].

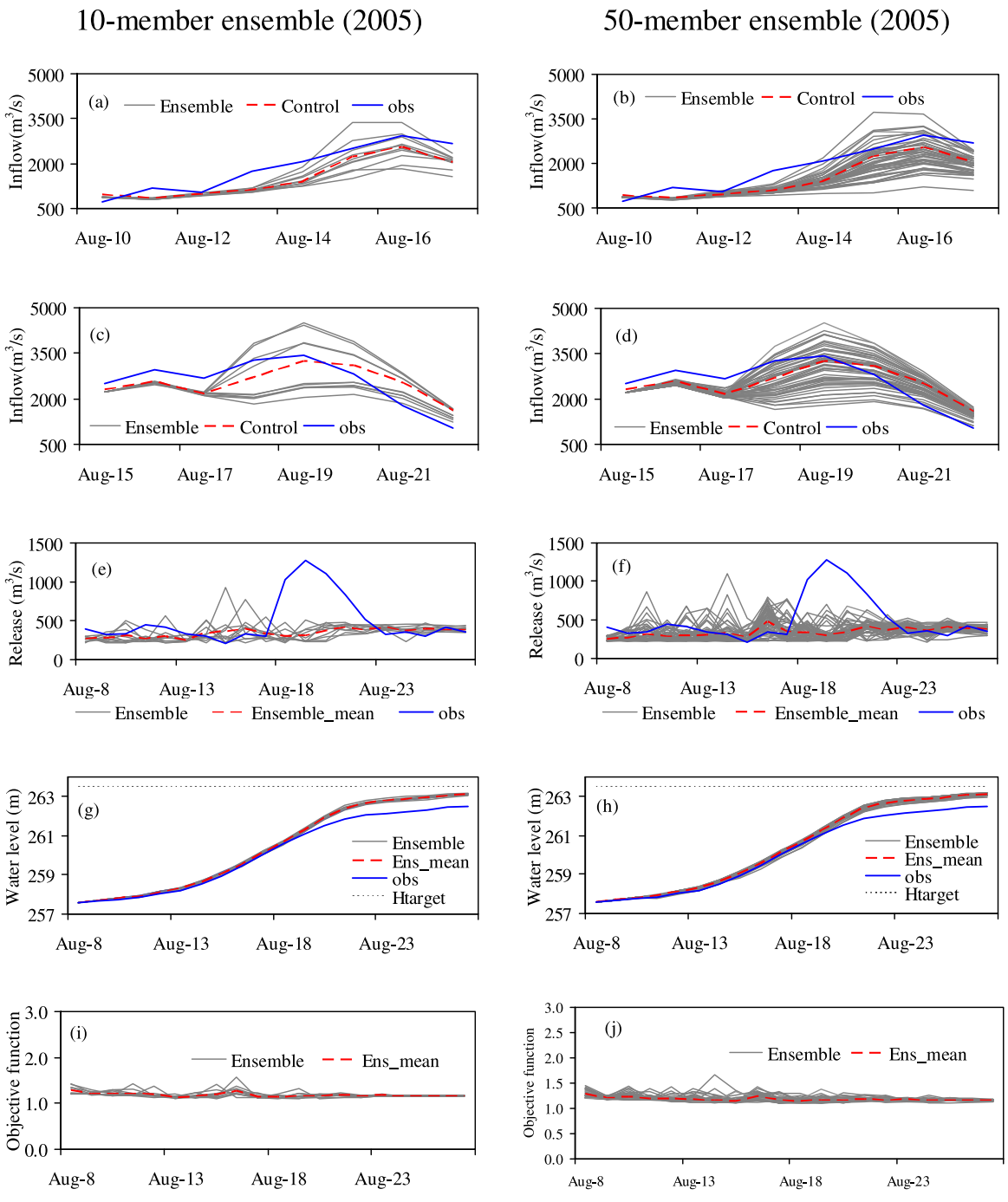

Figure 13. Same as Figure 11, but for (left) the 10-member ensemble results and (right) the 50-member ensemble results from 8 to 27 August 2005.

The ensemble average absolute error (AAE) [*Pappenberger et al.*, 2009; *Grimit and Clifford*, 2007] is defined as follows:

$$\mathrm{AAE} = \frac{1}{m}\sum_{i=1}^{m}|x_i - x_o|, \tag{31}$$

where m is the ensemble size, x_i is the ith ensemble forecast, and x_o is the observed value.

[63] Figure 13 compares the 10-member and 50-member ensemble optimization results. Figures 13a and 13b (Figures 13c and 13d) show the ensemble forecast reservoir inflows during flood rising (recession) stage for 10 and 50 ensemble members, respectively. In general, all the ensemble inflows cover the flood sceneries (especially peak values) with 50-member results revealing a broader range than 10-member results. The flood peaks in Figures 13a and 13b are between 1834 and 3360 m^3 s^{-1} and between 1212 and 3662 m^3 s^{-1}, respectively (observation is 2950 m^3 s^{-1}). The flood peaks in Figures 13c and 13d are between 2038 and 4483 m^3 s^{-1} and between 1792 and 4521 m^3 s^{-1}, respectively (observation is 3429 m^3 s^{-1}). The PO of

ensemble inflow forecast is 0.625 and 0.500 (not shown) for 10 members and 50 members, respectively.

[64] Figure 14 shows the ensemble spread (Figures 14a and 14b) and AAE (Figures 14c and 14d) for 10-member and 50-member ensemble inflows. In general, the ensemble spread for 50-member ensemble (346 $m^3 s^{-1}$) is larger than that for 10 members (307 $m^3 s^{-1}$). The mean AAE for 50 members (486 $m^3 s^{-1}$) shows lower value that that for 10 members (505 $m^3 s^{-1}$).

[65] Figures 13e and 13f give the optimized reservoir releases for 10 and 50 ensemble members, respectively. The different ensemble sizes generate different release schedule especially during the flood rising period. The maximum releases are 928 and 1097 $m^3 s^{-1}$ for the 10- and 50-member ensemble sizes, respectively. The ensemble mean release schedules are comparable with the maximum release equal 413 and 477 $m^3 s^{-1}$ for 10- and 50-member ensemble sizes, respectively.

[66] Figures 13g and 13h plot the optimized reservoir water levels for the 10- and 50-member ensemble sizes, respectively. All of the optimized water levels are lower than the maximum water level requirement (263.50 m) and higher than the measured values (262.51 m). The water level variation process is different for the two ensemble results, but the end water level is identical (263.12 m, ensemble mean) for both of the 10- and 50-member ensemble results.

[67] Figures 13i and 13j illustrate the optimized objective functions for the 10- and 50-member ensemble sizes, respectively. The objective function ranges for the 50-member ensemble results are wider than 10-member ensemble results, but the ensemble mean values are comparable (both between 1.15 and 1.28).

[68] In summary, the system running with 50-member ensembles generates wider ranges of inflows and releases than 10-member ensemble results. The ensemble mean releases and end water levels are comparable for both cases. The RMSE for the ensemble mean inflow errors is 466 and 480 $m^3 s^{-1}$ for 50 and 10 members, respectively. This result indicates that the 50-member ensembles show slightly better results than that for 10-member ensembles in representing inflow uncertainties.

5.2. Critical Events

[69] This section discusses the performance of the system under critical situations. First, the system (30 ensemble members) is running with the target water levels of 262.50 m and 261.50 m (upper bound of limited water level is 263.50 m) using 2005 flood event. Second, the system is tested for the 2001 flood event with the target water level equal to 263.50 m. This flood is characterized by the high flood peak (5328 $m^3 s^{-1}$). Because JMA's operational NWPs are only available after May 2002, the system is fed with ERA-Interim data in 2001.

[70] Figures 15a, 15c and 15e demonstrate the Fengman reservoir optimization results with the target water level of 262.50 m for 2005 flood event. The optimized maximum release for ensemble mean (around 970 $m^3 s^{-1}$) occurs on 16 August 2005 (Figure 15a), while the observed inflow peak (3429 $m^3 s^{-1}$) is on 19 August 2005. This result is reasonable since the system takes advantage of 8 days QPF forecasting information for releases optimizations. The optimized release peak occurs before the reservoir inflow peak reached, while the actual operations fail in predischarge. Figure 15c shows the optimized reservoir water levels. All of the water levels are increasingly close to the target water level (262.50 m) at the end of optimization with the ensemble mean equal to 262.37 m.

[71] Figures 15b, 15d, and 15f draw the Fengman reservoir optimization results with the target water level of 261.50 m for 2005 flood event. The optimized maximum release for ensemble mean is 1410 $m^3 s^{-1}$ on 16 August 2005, and it decreases to 894 $m^3 s^{-1}$ during the reservoir inflow peak (19 August 2005, 3429 $m^3 s^{-1}$). The ensemble mean water level is 261.45 m at the end of optimization (target level is 261.50 m). For both cases (target level of 262.50 m and 261.50 m), the objective functions satisfy the constraint requirements (Figures 15e and 15f).

[72] Figure 16 shows the reservoir optimization results for 2001 flood event (25 July to 25 August) fed with ERA-Interim data. The optimized maximum reservoir release (1199 $m^3 s^{-1}$) is lower than the observation (1922 $m^3 s^{-1}$). The optimized end water level (261.36 m) is higher than the observed value (259.26 m) but lower than the constraint

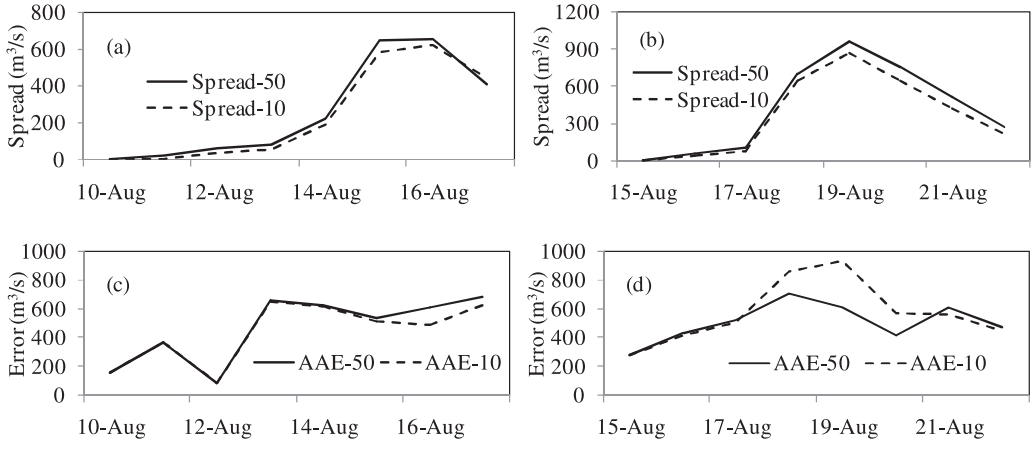

Figure 14. Comparison of (a and b) ensemble spread and (c and d) average absolute error (AAE) for 10-member and 50-member ensemble inflow forecasts (left) from 10 to 17 August 2005 (flood rising) and (right) from 15 to 22 August 2005 (flood recession).

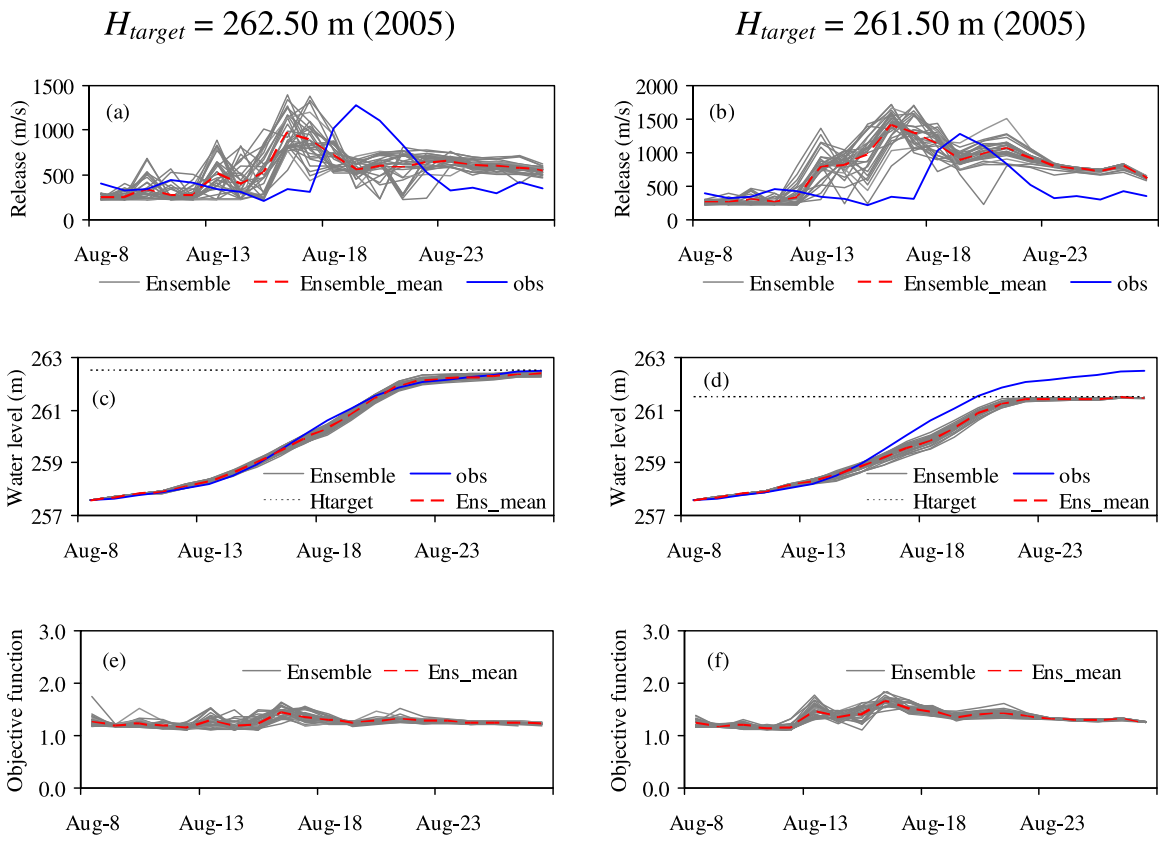

Figure 15. Same as Figure 11, but for (a and b) reservoir release, (c and d) water level, and (e and f) objective function from 8 to 27 August 2005 with lower target reservoir water levels: (left) 262.50 and (right) 261.50 m.

level (263.50 m). The objective functions also satisfy the constraint requirements (Figure 16b). These results reveal the system's capability of directing real-time operation under critical situation.

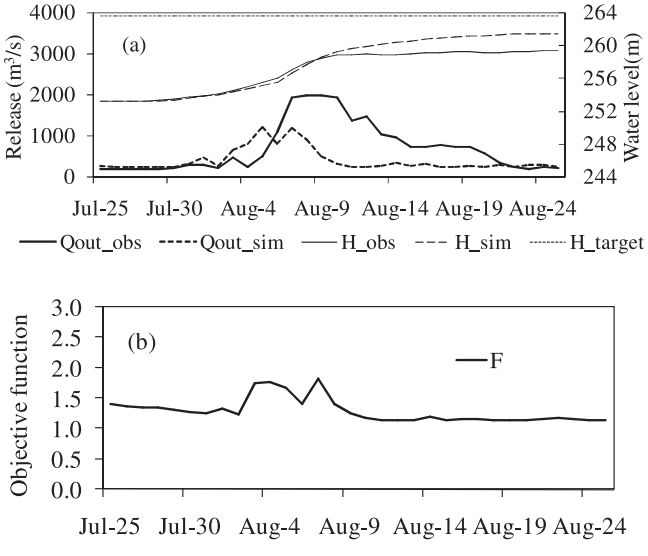

Figure 16. Same as Figure 10, but for (a) optimized reservoir release and water level and (b) objective function for the 2001 flood event (from 25 July to 25 August). The system is forced by ERA-Interim data.

5.3. The Feasibility of Practical Operation

[73] The running time for 8 day lead time optimization with 30 ensemble members is approximately 33 min using a 3 GHz CPU personal computer. The total execution time (33 min) includes ensemble streamflow forecasting (29.6 min, 89.7%), hydrological states updating (3.3 min, 10.0%), and reservoir release optimization (0.09 min, 0.3%) time. The relatively high cost of ensemble streamflow forecasting is due to the fine resolution of WEB-DHM model (3 km and 1 h). The time can be reduced dramatically using a parallel computing system. The JMA NWP data issued interval is 24 h. Therefore, the system is feasible for real-time reservoir operation.

[74] The model parameters contain reservoir characteristic parameters, hydrological model (WEB-DHM) parameters, and initial and target water levels. The reservoir characteristics include reservoir characteristic water levels, reservoir storage capacity curve, discharging curve, and downstream flood control requirements. These parameters are depending on the reservoirs. The WEB-DHM parameters include soil surface saturated hydraulic conductivity; anisotropy ratio, maximum surface water storage, and van Genuchen's parameter [see *Wang et al.*, 2011]. They can be calibrated before embedding into the operation system. The reservoir initial and target water levels are set by reservoir operators. Therefore, the system is easy to operate even though the reservoir operators have not been involved in the formulation and development of the simulation and optimization models.

6. Conclusions

[75] Despite the fact that considerable progress has been made on reservoir operation, it has still been very slow in finding its way into practice because of the uncertainties in streamflow forecasting and the complexity of the operation models [*Yeh*, 1985; *Russell and Campbell*, 1996; *Chang et al.*, 2005]. The objective of this study was to propose an ensemble prediction-based reservoir optimization system (EPROS) considering the QPF errors. The EPROS is developed from the prototype of DRESS model [*Saavedra Valeriano et al.*, 2010], but enhanced features were added with a wider application in a semiarid basin (northeast China) using global data sets and longer QPF. The extreme floods (flood seasons) and long-term serious drought (non-flood seasons) often happen in this region. The EPROS system consists of three submodels: a QPF perturbation model, a hydrological prediction model (WEB-DHM) and a reservoir optimization model. The EPROS objectives include minimizing the maximum reservoir water level (for reservoir and upstream safety), minimizing the downstream flood peak, and minimizing the difference between the optimized and the target water levels at the end of operation (for future water use).

[76] The main improvements of EPROS include (1) improving the QPF intensity error definition method (to avoid the compensation of inaccurate forecast) and defining the perturbation weight using intensity error and location error objectively instead of using proposed zones and look up table, (2) comparing the performance of ensemble QPFs generated by EPROS with JMA's ensemble NWPs using probability-based measures (e.g., CRPS and RH), (3) updating the hydrological status of WEB-DHM at each time step continuously, (4) improving the reservoir optimization model by normalizing the objectives to the same magnitude order (to improve the stability of optimization), as well as adding a new objective (reservoir and upstream flood control safety), a new constraint (release amplitude) and a dynamic penalty function, (5) embedding all of the JMA NWPs' (global scale) atmospheric forcing parameters (QPF, winds, air temperature, relative humidity, and surface pressure) into EPROS, (6) generating the ensemble reservoir status (water levels and releases) for real-time decision making, and (7) analyzing the sensitivity of reservoir efficiency to ensemble size and the performance of EPROS under critical events. The reservoir (and upstream) flood control safety is essential for actual reservoir operation. The release amplitude constraint is important for protecting the downstream channels and turbine. The dynamic penalty function is efficient for solving multi-constraint optimization problem. The EPROS fed with global scale forecasts makes it feasible to be applied to other river basins in the world.

[77] The EPROS system has been evaluated on Fengman reservoir in northeast China for the flood events in 2004 (from 17 July to 15 August) and 2005 (from 8 to 27 August). The initial reservoir water levels of the optimization system were set as the observed values and the target water levels were set as 263.50 m (the upper bound of limit water level). For both events, the QPFs capture the major rainfall event but the accuracy decreases with the lead time increasing from 1 to 8 days. The ensemble QPFs generated by EPROS are comparable to that obtained from JMA by measuring their performances using CRPS and RH. The system was driven by deterministic QPFs and perturbed QPFs. The ensemble-based streamflow predictions reduced the uncertainties of single prediction by generating multiple (e.g., 30 members) streamflow sceneries. All of the ensemble release peaks were lower than the observed values. The ensemble mean release peaks were 785 $m^3 s^{-1}$ for 2004 and 462 $m^3 s^{-1}$ for 2005, while the observed release peaks were 1952 $m^3 s^{-1}$ for 2004 and 1278 $m^3 s^{-1}$ for 2005. As a result, the ensemble mean end water levels (261.51 m for 2004 and 263.13 m for 2005) were higher than the observations (257.44 m for 2004 and 262.51 m for 2005). This is very important for alleviating long-term water shortage problem for this semiarid region. The optimized maximum reservoir water levels also satisfied the constraint requirements (263.50 m), which are important for reservoir and upstream safety.

[78] In general, the system is not sensitive to the ensemble sizes. Although 50-member ensemble generated wider range for streamflows and releases than 10-member ensemble results, the ensemble mean values (e.g., water levels, releases) were comparable. The system's capability was also evaluated under critical situations by decreasing the maximum water level from 263.50 m to 262.50 m. The system was robust in reducing downstream flood peak and decreasing maximum reservoir water level, as well as decreasing the discrepancies between optimized end water level and target water level by predischarges before flood peaks reached. The system is of high efficiency and easy to operate. It can provide not only deterministic release schedules (ensemble mean) but also the uncertainty range (ensemble range) for practical operation.

[79] The research would promote the practical applications of QPFs and provide a blueprint for real-time reservoir operation for other river basins. Further efforts are encouraged to examine the applicability of the system to different reservoirs under different meteorological conditions. Because the observed discharge data are embedded to the EPROS system in the present work, it is also necessary to expand the single-reservoir model to multireservoir optimization when the precipitation data are available for the Hongshi basin. Besides, mesoscale NWP models (e.g., weather research and forecasting model) are expected to obtain more reliable meteorological predictions with finer resolutions (both spatial and temporal) for the EPROS system.

[80] **Acknowledgments.** The authors gratefully acknowledge financial support provided by the China Scholarship Council. The authors are deeply indebted to Florian Pappenberger (ECMWF) and two anonymous reviewers for their valuable comments and suggestions that greatly improved the quality of this paper. We also thank Kitsuregawa Laboratory at the Institute of Industrial Science, University of Tokyo, for providing JMA NWP data. The authors sincerely thank Koji Terasaki, who provided guidance in extracting JMA ensemble NWP data. The Fengman reservoir operation data were obtained from the Fengman Hydropower Plant. This study was financially supported by the National Natural Science Foundation of China (grants 50809011 and 50909012) and the Hundred Talents Program of the Chinese Academy of Sciences.

References

Asian Development Bank (2002), Report and recommendation of the president to the board of directors on a proposed loan to the People's Republic of China for the Songhua River flood management sector project, *RRP PRC 33437*, Asian Development Bank, Manila.

Barakat, S., and H. Ibrahim (2011), Application of shuffled complex evolution global optimization technique in the design of truss structures, in *2011 4th International Conference of Modeling, Simulation and Applied Optimization (ICMSAO), Kuala Lumpur*, pp. 1–6, IEEE Press, Piscataway, N. J., doi:10.1109/ICMSAO.2011.5775590.

Boyle, D. P., H. V. Gupta, and S. Sorooshian (2000), Toward improved calibration of hydrological models: Combining the strengths of manual and automatic methods, *Water Resour. Res.*, *36*(12), 3663–3674, doi:10.1029/2000WR900207.

Buizza, R., and T. N. Palmer (1995), The singular-vector structure of the atmospheric global circulation, *J. Atmos. Sci.*, *52*, 1434–1456, doi:10.1175/1520-0469(1995)052<1434:TSVSOT>2.0.CO;2.

Buizza, R., P. L. Houtekamer, G. Pellerin, Z. Toth, Y. Zhu, and M. Wei (2005), A comparison of the ECMWF, MSC, and NCEP global ensemble prediction systems, *Mon. Weather Rev.*, *133*(5), 1076–1097, doi:10.1175/MWR2905.1.

Cai, X., M. W. Rosegrant, and C. Ringler (2003), Physical and economic efficiency of water use in the river basin: Implications for efficient water management, *Water Resour. Res.*, *39*(1), 1013, doi:10.1029/2001WR000748.

Candille, G., C. Côté, P. L. Houtekamer, and G. Pellerin (2007), Verification of an ensemble prediction system against observations, *Mon. Weather Rev.*, *135*(7), 2688–2699.

Chakraborty, A. (2010), The skill of ECMWF medium-range forecasts during the Year of Tropical Convection 2008, *Mon. Weather Rev.*, *138*, 3787–3805, doi:10.1175/2010MWR3217.1.

Chang, Y. T., L. C. Chang, and F. J. Chang (2005), Intelligent control for modeling of real-time reservoir operation, part II: Artificial neural network with operating rule curves, *Hydrol. Processes*, *19*(7), 1431–1444.

Chu, W., X. Gao, and S. Sorooshian (2010), Improving the shuffled complex evolution scheme for optimization of complex nonlinear hydrological systems: Application to the calibration of the Sacramento soil-moisture accounting model, *Water Resour. Res.*, *46*, W09530, doi:10.1029/2010WR009224.

Clark, M. P., and L. E. Hay (2004), Use of medium-range numerical weather prediction model output to produce forecasts of streamflow, *J. Hydrometeorol.*, *5*, 15–32.

Clark, M. P., S. Gangopadhyay, L. E. Hay, B. Rajagopalan, and R. Wilby (2004), The Schaake shuffle: A method for reconstructing space-time variability in forecasted precipitation and temperature fields, *J. Hydrometeorol.*, *5*, 243–262.

Cloke, H. L., and F. Pappenberger (2009), Ensemble flood forecasting: A review, *J. Hydrol.*, *375*(3–4), 613–626, doi:10.1016/j.jhydrol.2009.06.005.

Crawford, T. M., and C. E. Duchon (1999), An improved parameterization for estimating effective atmospheric emissivity for use in calculating daytime downwelling longwave radiation, *J. Appl. Meteorol.*, *38*, 474–480, doi:10.1175/1520-0450(1999)038<0474:AIPFEE>2.0.CO;2.

Croley, T. E., II, and K. N. Raja Rao (1979), Multiobjective risks in reservoir operation, *Water Resour. Res.*, *15*(4), 807–814, doi:10.1029/WR015i004p00807.

Cui, B., Z. Toth, Y. J. Zhu, and D. C. Hou (2011), Bias correction for global ensemble forecast, *Weather Forecast.*, *27*, 396–410, doi:http://dx.doi.org/10.1175/WAF-D-11-00011.1.

Day, G. N. (1985), Extended streamflow forecasting using NWSRFS, *J. Water Resour. Plann. Manage.*, *111*, 157–170, doi:10.1061/(ASCE)0733-9496(1985)111:2(157).

Dee, D. P., et al., (2011), The ERA-Interim reanalysis: Configuration and performance of the data assimilation system, *Q. J. R. Meteorol. Soc.*, *137*, 553–597, doi:10.1002/qj.828.

Dietrich, J., S. Trepte, Y. Wang, A. H. Schumann, F. Voß, F. B. Hesser, and M. Denhard (2008), Combination of different types of ensembles for the adaptive simulation of probabilistic flood forecasts: Hindcasts for the Mulde 2002 extreme event, *Nonlinear Proc. Geophys.*, *15*, 275–286.

Dorigo, M., V. Maniezzo, and A. Colorni (1996), Ant system: Optimization by a colony of cooperating ants, *IEEE Trans. Syst. Man Cybern.*, *26*(1), 29–42, doi:10.1109/3477.484436.

Duan, Q., S. Sorooshian, and V. K. Gupta (1992), Effective and efficient global optimization for conceptual rainfall-runoff models, *Water Resour. Res.*, *28*(4), 1015–1031, doi:10.1029/91WR02985.

Duan, Q., V. K. Gupta, and S. Sorooshian (1993), Shuffled complex evolution approach for effective and efficient global minimization, *J. Optim. Theory. Appl.*, *76*(3), 501–521, doi:10.1007/BF00939380.

Duan, Q., S. Sorooshian, and V. K. Gupta (1994), Optimal use of the SCE-UA global optimization method for calibrating watershed models, *J. Hydrol.*, *158*, 265–284, doi:10.1016/0022-1694(94)90057-4.

Faber, B., and J. Stedinger (2001), Reservoir optimization using sampling SDP with ensemble streamflow prediction (ESP) forecasts, *J. Hydrol.*, *249*, 113–133, doi:10.1016/S0022-1694(01)00419-X.

Fan, Y., and H. van den Dool (2011), Bias correction and forecast skill of NCEP GFS ensemble week-1 and week-2 precipitation, 2-m surface air temperature, and soil moisture forecasts, *Weather Forecast.*, *26*, 355–370, doi:10.1175/WAF-D-10-05028.1.

Food and Agriculture Organization (2003), *Digital soil map of the world and derived soil properties, land and water digital media series, revision 1 [CD-ROM]*, Rome.

Frogner, I.-L., and T. Iversen (2001), Targeted ensemble prediction for northern Europe and parts of the North Atlantic Ocean, *Tellus, Ser. A*, *53*(1), 35–55, doi:10.1034/j.1600-0870.2001.01132.x.

Goldberg, D. (1989), *Genetic Algorithms in Search, Optimization and Machine Learning*, Addison-Wesley Longman, Boston, Mass.

Grimit, E. P., and F. M. Clifford (2007), Measuring the ensemble spread–error relationship with a probabilistic approach: Stochastic ensemble results, *Mon. Weather Rev.*, *135*, 203–221, doi:10.1175/MWR3262.1.

Hamill, T. M. (2001), Interpretation of rank histograms for verifying ensemble forecasts, *Mon. Weather Rev.*, *129*, 550–560, doi:10.1175/1520-0493(2001)129<0550:IORHFV>2.0.CO;2.

Hamill, T. M., C. Snyder, and R. E. Morss (2000), A comparison of probabilistic forecasts from bred, singular-vector, and perturbed observation ensembles, *Mon. Weather Rev.*, *128*, 1835–1851.

Hersbach, H. (2000), Decomposition of the continuous ranked probability score for ensemble prediction systems, *Weather Forecast.*, *15*, 559–570, doi:10.1175/1520-0434(2000)015<0559:DOTCRP>2.0.CO;2.

Houtekamer, P. L., L. Lefaivre, J. Derome, H. Ritchie, and H. L. Mitchell (1996), A system simulation approach to ensemble prediction, *Mon. Weather Rev.*, *124*, 1225–1242, doi:10.1175/1520-0493(1996)124<1225:ASSATE>2.0.CO;2.

Hsu, N.-S., and C.-C. Wei (2007), A multipurpose reservoir real-time operation model for flood control during typhoon invasion, *J. Hydrol.*, *336*, 282–293, doi:10.1016/j.jhydrol.2007.01.001.

Intergovernmental Panel on Climate Change (2007), *Climate Change 2007: Climate Change Impacts, Adaptation and Vulnerability, Summary for Policymakers*, World Meteorol. Organ., Geneva, Switzerland.

Japan Meteorological Agency (JMA) (2007), Outline of the operational forecast and analysis system of the Japan Meteorological Agency, appendix to *WMO technical progress report on the global data-processing and forecasting system and numerical weather prediction*, Japan Meteorological Agency, Tokyo. [Available at http://www.jma.go.jp/jma/jma-eng/jma-center/nwp/outline-nwp/index.htm.]

Johnson, S. A., J. R. Stedinger, and K. Staschus (1991), Heuristic operating policies for reservoir system simulation, *Water Resour. Res.*, *27*(5), 673–685, doi:10.1029/91WR00320.

Kennedy, J., and R. C. Eberhart (1995), Particle swarm optimization, in *Proceedings of IEEE International Conference on Neural Networks*, pp. 1942–1948, IEEE Press, Piscataway, N. J., doi:10.1109/ICNN.1995.488968.

Khu, S. T., and H. Madsen (2005), Multiobjective calibration with Pareto preference ordering: An application to rainfall–runoff model calibration, *Water Resour. Res.*, *41*, W03004, doi:10.1029/2004WR003041.

Krzysztofowicz R. (2001), The case for probabilistic forecasting in hydrology, *J. Hydrol.*, *249*, 2–9, doi:10.1016/S0022-1694(01)00420-6.

Kumar, D., and M. Reddy (2006), Ant colony optimization for multipurpose reservoir operation, *Water Resour. Manage.*, *20*(6), 879–898, doi:10.1007/s11269-005-9012-0.

Labadie, J. W. (2004), Optimal operation of multireservoir system: State-of-the-art review, *J. Water. Resour. Plann. Manage.*, *130*, 93–111, doi:10.1061/(ASCE)0733-9496(2004)130:2(93).

Lin, C., S. Vasić, A. Kilambi, B. Turner, and I. Zawadzki (2005), Precipitation forecast skill of numerical weather prediction models and radar nowcasts, *Geophys. Res. Lett.*, *32*, L14801, doi:10.1029/2005GL023451.

Lorenz, E. N. (1969), The predictability of a flow which contains many scales of motion, *Tellus*, *21*, 289–307, doi:10.1111/j.2153-3490.1969.tb00444.x.

Mascaro, G., E. Vivoni, and R. Deidda (2010), Implications of ensemble quantitative precipitation forecast errors on distributed streamflow forecasting, *J. Hydrometeorol.*, *11*(1), 69–86, doi:10.1175/2009JHM1144.1.

Michalewicz, Z. (1995), Genetic algorithms, numerical optimization, and constraints, in *Proceedings of the Sixth International Conference on Genetic Algorithms*, pp. 151–158, Morgan Kaufmann, San Francisco.

Molteni, F., R. Buizza, T. N. Palmer, and T. Petroliagis (1996), The ECMWF ensemble prediction system: Methodology and validation, *Q. J. R. Meteorol. Soc.*, *122*, 73–119, doi:10.1002/qj.49712252905.

Myneni, R. B., R. R. Nemani, and S. W. Running (1997), Algorithm for the estimation of global land cover, LAI and FPAR based on radiative transfer models, *IEEE Trans. Geosci. Remote Sens.*, *35*, 1380–1393.

Nash, J. E., and J. V. Sutcliffe (1970), River flow forecasting through conceptual models part I—A discussion of principles, *J. Hydrol.*, *10*, 282–290, doi:10.1016/0022-1694(70)90255-6.

Ngo, L. L., H. Madsen, and D. Rosbjerg (2007), Simulation and optimization modelling approach for operation of the Hoa Binh reservoir, Vietnam, *J. Hydrol.*, *336*, 269–281, doi:10.1016/j.jhydrol.2007.01.003.

Niewiadomska-Szynkiewicz, E., K. Malinowski, and A. Karbowski (1996), Predictive methods for real-time control of flood operation of a multireservoir system: Methodology and comparative study, *Water Resour. Res.*, *32*(9), 2885–2895, doi:10.1029/96WR01443.

Oliveira, R., and D. P. Loucks (1997), Operating rules for multireservoir systems, *Water Resour. Res.*, *33*(4), 839–852, doi:10.1029/96WR03745.

Pappenberger, F., and R. Buizza (2009), The skill of ECMWF precipitation and temperature predictions in the Danube Basin as forcings of hydrological models, *Weather Forecast.*, *24*(3), 749–766, doi:10.1175/2008WAF2222120.1.

Pappenberger, F., A. Ghelli, R. Buizza, and K. Bodis (2009), The skill of probabilistic precipitation forecasts under observational uncertainties within the generalized likelihood uncertainty estimation framework for hydrological applications, *J. Hydrometeorol.*, *10*(3), 794–806.

Parton, W. J., and J. A. Logan (1981), A model for diurnal variation in soil and air temperature, *Agric. Meteorol.*, *23*, 205–216, doi:10.1016/0002-1571(81)90105-9.

Ramos, M. H., J. Bartholmes, and J. Thielen (2007), Development of decision support products based on ensemble weather forecasts in the European flood alert system, *Atmos. Sci. Lett.*, *8*, 113–119, doi:10.1002/asl.161.

Reddy, M. J., and D. N. Kumar (2007), Multi-objective particle swarm optimization for generating optimal trade-offs in reservoir operation, *Hydrol. Processes*, *21*(21), 2897–2909, doi:10.1002/hyp.6507.

Roulin, E., and S. Vannitsem (2005), Skill of medium-range hydrological ensemble predictions, *J. Hydrometeorol.*, *6*, 729–744, doi:10.1175/JHM436.1.

Russell, S. O., and P. F. Campbell (1996), Reservoir operating rules with fuzzy programming, *J. Water Resour. Plann. Manage.*, *122*(3), 165–170.

Saavedra Valeriano, O. C., T. Koike, K. Yang, T. Graf, X. Li, L. Wang, and X. Han (2010a), Decision support for dam release during floods using a distributed biosphere hydrological model driven by quantitative precipitation forecasts, *Water Resour. Res.*, *46*, W10544, doi:10.1029/2010WR009502.

Saavedra Valeriano, O. C., T. Koike, K. Yang, and D. W. Yang (2010b), Optimal dam operation during flood season using a distributed hydrological model and a heuristic algorithm, *J. Hydrol., Eng.*, *15*(7), 580–586, doi:10.1061/(ASCE)HE.1943-5584.0000212.

Saito, K., J. I. Ishida, K. Aranami, T. Hara, T. Segawa, M. Narita, and Y. Honda (2007), Nonhydrostatic atmospheric models and operational development at JMA, *J. Meteorol. Soc. Jpn.*, *85B*, 271–304, doi:10.2151/jmsj.85B.271.

Schaake, J. C., K. Franz, V. Bradley, and R. Buizza (2006), The Hydrologic Ensemble Prediction Experiment (HEPEX), *Hydrol. Earth Syst. Sci.*, *3*, 3321–3332, doi:10.1175/BAMS-88-10-1541.

Schaake, J. C., J. Demargne, R. Hartman, M. Mullusky, E. Welles, L. Wu, H. Herr, X. Fan, D.-J. Seo (2007), Precipitation and temperature ensemble forecasts from single-value forecasts, *Hydrol. Earth Syst. Sci. Discuss.*, *4*, 655–717.

Sellers, P. J., D. A. Randall, G. J. Collatz, J. A. Berry, C. B. Field, D. A. Dazlich, C. Zhang, G. D. Collelo, and L. Bounoua (1996a), A revised land surface parameterization (SiB2) for atmospheric GCMs, Part I: Model formulation, *J. Clim.*, *9*(4), 676–705.

Sellers, P. J., S. O. Los, C. J. Tucker, C. O. Justice, D. A. Dazlich, G. J. Collatz, and D. A. Randall (1996b), A revised land surface parameterization (SiB2) for atmospheric GCMs, part II: the generation of global fields of terrestrial biosphysical parameters from satellite data, *J. Clim.*, *9*, 706–737.

Sorooshian, S., Q. Duan, and V. K. Gupta (1993), Calibration of rainfall-runoff models: Application of global optimization to the Sacramento soil moisture accounting model, *Water Resour. Res.*, *29*(4), 1185–1194, doi:10.1029/92WR02617.

Stedinger, J. R., B. F. Sule, and D. P. Loucks (1984), Stochastic dynamic programming models for reservoir operation optimization, *Water Resour. Res.*, *20*(11), 1499–1505, doi:10.1029/WR020i011p01499.

Tejada-Guibert, J. A., S. A. Johnson, and J. R. Stedinger (1995), The value of hydrologic information in stochastic dynamic programming models of a multireservoir system, *Water Resour. Res.*, *31*(10), 2571–2579, doi:10.1029/95WR02172.

Thielen, J., J. Bartholmes, M.-H. Ramos, and A. de Roo (2009), The European Flood Alert System—Part 1: Concept and development, *Hydrol. Earth Syst. Sci.*, *13*(2), 125–140.

Toth, Z., and E. Kalnay (1993), Ensemble forecasting at NMC: The generation of perturbations, *Bull. Am. Meteorol. Soc.*, *74*(12), 2317–2330.

Toth, Z., and E. Kalnay (1997), Ensemble forecasting at NCEP and the breeding method, *Mon. Weather Rev.*, *125*, 3297–3319, doi:10.1175/1520-0493(1997)125<3297:EFANAT>2.0.CO;2.

Turner, M. R. J., J. P. Walker, and P. R. Oke (2008), Ensemble member generation for sequential data assimilation, *Remote Sens. Environ.*, *112*, 1421–1433, doi:10.1016/j.rse.2007.02.042.

Vrugt, J. A., H. V. Gupta, W. Bouten, and S. Sorooshian (2003), A shuffled complex evolution metropolis algorithm for optimization and uncertainty assessment of hydrologic model parameters, *Water Resour. Res.*, *39*(8), 1201, doi:10.1029/2002WR001642.

Wang, B. D., H. C. Zhou, and C. T. Cheng (1994), Fuzzy optimizing approach to flood operation of multiobjective cascade reservoirs [in Chinese], *J. Hydraul. Eng.*, *2*, 31–39, 45.

Wang, F., L. Wang, T. Koike, H. Zhou, K. Yang, A. Wang, and W. Li (2011), Evaluation and application of a fine-resolution global data set in a semiarid mesoscale river basin with a distributed biosphere hydrological model, *J. Geophys. Res.*, *116*, D21108, doi:10.1029/2011JD015990.

Wang, L., T. Koike, K. Yang, T. J. Jackson, R. Bindlish, and D. W. Yang (2009a), Development of a distributed biosphere hydrological model and its evaluation with the Southern Great Plains Experiments (SGP97 and SGP99), *J. Geophys. Res.*, *114*, D08107, doi:10.1029/2008JD010800.

Wang, L., T. Koike, K. Yang, and P. Yeh (2009b), Assessment of a distributed biosphere hydrological model against streamflow and MODIS land surface temperature in the upper Tone River Basin, *J. Hydrol.*, *377*, 21–34, doi:10.1016/j.jhydrol.2009.08.005.

Wang, L., T. Koike, D. W. Yang, and K. Yang (2009c), Improving the hydrology of the Simple Biosphere Model and its evaluation within the framework of a distributed hydrological model, *Hydrol. Sci. J.*, *54*(6), 989–1006, doi:10.1623/hysj.54.6.989.

Werner, K., D. Brandon, M. Clark, and S. Gangopadhyay (2005), Incorporating medium-range numerical weather model output into the ensemble streamflow prediction system of the National Weather Service, *J. Hydrometeorol.*, *6*, 101–114.

Wu, L. M., D.-J. Seo, J. Demargne, J. D. Brown, S. Z. Cong, and J. Schaake (2011), Generation of ensemble precipitation forecast from single-valued quantitative precipitation forecast for hydrologic ensemble prediction, *J. Hydrol.*, *399*, 281–298, doi:10.1016/j.jhydrol.2011.01.013.

Yamaguchi, M., R. Sakai, M. Kyoda, T. Komori, and T. Kadowaki (2009), Typhoon ensemble prediction system developed at the Japan Meteorological Agency, *Mon. Weather Rev.*, *137*, 2592–2604, doi:10.1175/2009MWR2697.1.

Yang, D. W., S. Herath, and K. Musiake (2002), A hillslope-based hydrological model using catchment area and width functions, *Hydrol. Sci. J.*, *47*(1), 49–65, doi:10.1080/02626660209492907.

Yang, D. W., T. Koike, and H. Tanizawa (2004a), Application of a distributed hydrological model and weather radar observations for flood management in the upper Tone River of Japan, *Hydrol. Processes*, *18*(16), 3119–3132, doi:10.1002/hyp.5752.

Yang, D. W., C. Li, G. H. Ni, and H. P. Hu (2004b), Application of a distributed hydrological model to the Yellow River Basin [in Chinese], *Acta Geogr. Sin.*, *59*(1), 143–154.

Yang, K., G. W. Huang, and N. Tamai (2001), A hybrid model for estimating global solar radiation, *Sol. Energy*, *70*(1), 13–22, doi:10.1016/S0038-092X(00)00121-3.

Yang, K., T. Koike, and B. S. Ye (2006), Improving estimation of hourly, daily, and monthly solar radiation by importing global data sets, *Agric. For. Meteorol.*, *137*(1–2), 43–55, doi:10.1016/j.agrformet.2006.02.001.

Yeh, W. W.-G. (1985), Reservoir management and operations models: A state-of- the-art review, *Water Resour. Res.*, *21*(12), 1797–1818, doi:10.1029/WR021i012p01797.

Yeh, W. W.-G., and L. Becker (1982), Multiobjective analysis of multireservoir operations, *Water Resour. Res.*, *18*(5), 1326–1336, doi:10.1029/WR018i005p01326.

Yeniay, Ö. (2005), Penalty function methods for constrained optimization with genetic algorithms, *Math. Comput. Appl.*, *10*(1), 45–56.

You, J.-Y., and X. Cai (2008), Hedging rule for reservoir operations: 1. A theoretical analysis, *Water Resour. Res.*, *44*, W01415, doi:10.1029/2006WR005481.